TÉCNICO LISBOA

BEHAVIOUR OF COMPOSITE PLATES UNDER COMPRESSION

Sven Stephan

Thesis to obtain the Master of Science Degree in

Naval Architecture and Marine Engineering

Examination Committee

President of the Jury: Prof. Yordan Garbatov
Supervisor: Prof. Carlos Guedes Soares
Vogal: Dr. Leigh Sutherland

July 2016

TÉCNICO LISBOA

DECLARAÇÃO

Eu **Sven Stephan**, aluno do Instituto Superior Técnico nº **ist179440**, autor da dissertação para obtenção do Grau de Mestre em **Engenharia e Arquitetura Naval**, com o título **Behaviour of Composite Plates under Compression** concedo ao Instituto Superior Técnico uma licença perpétua, mas não exclusiva, para utilizar esta dissertação para fins de ensino ou investigação e autorizo-o a inseri-la, bem como ao seu resumo alargado, em formato pdf, na sua página da internet, com endereço www.tecnico.ulisboa.pt de modo a permitir a sua divulgação junto de todos os que acedam àquela página, e, com o mesmo propósito de divulgação, a responder favoravelmente aos pedidos de instituições de ensino ou de investigação e Centros de Documentação ou Bibliotecas, remetendo-lhes aqueles mesmos ficheiros em formato pdf, mas fazendo uma expressa menção, seja na sua página na internet seja quando da remessa atrás referida, à obrigação de quem assim aceda àquela minha dissertação e respectivo resumo alargado em salvaguardar os meus direitos de autor sobre estes documentos, que me são conferidos pelo Código do Direito de Autor e dos Direitos Conexos.

Lisboa, a 14 de Julho de 2016

O aluno n.º 79440

_____

(Sven Stephan)

This page is intentionally left blank

In memory of Peter Jürgen Stephan

This page is intentionally left blank

ACKNOWLEDGEMENTS

First and foremost, I would like to express my gratitude and appreciation to Navid Kharghani for his co-operation and help as my guide right from the inception of the problem to the final preparation of my master thesis. His profound knowledge of the presented subject and will to discuss made the submission of this work possible.

I express my sincere thanks and appreciation to Professor Carlos Guedes Soares for his guidance, support and help during the time of the entire master degree.

Furthermore, I want to thank all my colleagues and friends for their support and the great times we have had.

Finally, I extend my gratitude to my mother Heike, my sister Anne and my girlfriend Laura for always standing by me and supporting me at all times.

Sven Stephan

This page is intentionally left blank

ABSTRACT

Composite materials are widely used throughout different engineering fields for lightweight or high performance structures. The commercial use of these industries required analyses of various structural components as plates for example. This thesis handles an investigation about rectangular composite plates under uniaxial compressive loading comparing analytical and numerical calculations and practical experiments for pre- and post-buckling behaviour. Further, finite element analyses and mesh size analyses were computed to explore the impact of variation in element types and mesh sizes in the outcome of the numerical computations.

Three different plate sizes were chosen. The boundary conditions of the glass reinforced plastic plate are clamped at the loaded edges and free at the unloaded edges (Clamped-Free-Clamped-Free). The analytical calculations were developed on basis of the Classical Laminated Plate Theory (CLPT) and the First-Order Shear Deformation Theory (FSDT) as mathematical program codes in *Maple*. Numerical computations done in the finite element method (FEM) were conducted in *Ansys*. Practical experiments are done in a laboratory by applying equal boundary conditions.

Comparisons of analytical, numerical and experimental results showed that the numerical method gives most accurate predictions, followed by FSDT, whilst CLPT is more suitable for thinner plates. However, all three approaches confirm experimental test result behaviour. The variation of element types revealed that lower order element types are sufficiently precise and are not as affected by mesh refinements. Generally recommended are element type *Solid 45* and *64* for uniaxial fibre direction composite plates, while *Solid 46*, as a layered element type, is in addition capable to be modelled in different fibre directions per layers.

Keywords: composite materials, plates, buckling, Finite Element Method, FSDT, CLPT, element type analysis, mesh size analysis.

This page is intentionally left blank

RESUMO

O uso dos compósitos laminados é muito adoptado em diferentes ramos de engenharia como aplicações leves ou de alto desempenho. O uso comercial destas indústrias requereu análises de vários componentes estruturais, tais como placas por exemplo. Esta tese ocupa-se da investigação sobre placas rectangulares compósitas sujeitas a cargas não axiais compressivas de modo a comparar de análises analiticas, numéricas e experimentais no comportamento pre- e pós-encurvadura.

Por isso, foram escolhidos três tamanhos diferentes de placas. No terminus da placa plástica reforçada com vidro as bordas com carga são fixadas, e soltas nas bordas sem carga (clamped-free-clamped-free).

Os cálculos analíticos foram desenvolvidos com base na Teoria Clássica de Placas Laminadas (CLPT) e a Teoria de Primeira Ordem da Deformaçao de Corte (FSDT) com códigos de programa matemáticas em *Maple*. Todos os cálculos numéricos foram feitas na base do Método dos Elementos Finitos realizado em *Ansys*. Além disso, os Tipos de elementos e as analises de dimensão de malha foram feita em Ansys. A parte prática foi feito num laboratório sob condições constantes.

Os resultados mostraram que o método numérico deu as previsões mais precisos, seguido por FSDT, enquanto CLPT é mais adequado para as placas mais finas. No entanto, todas as três abordagens confirmam os resultados dos testes experimentais. A variação de tipos de elementos revelou que os elementos de ordem inferior são suficientemente precisos e não são tão afetados por refinamentos de dimensão de malha. Geralmente recomendado são os elementos do Tipo de *Solid 45* e *64* para placas de compósitos de fibra de direção uniaxiais, enquanto *Solid 46*, como um tipo de elemento em camadas, é capaz de ser modelado em diferentes direções fibra por camadas.

Palavras chave : materiais compósitos, encurvadura das placas, método dos elementos finitos, FSDT, CLPT, analise de dimensão de malha, analise de Tipo dos elementos finitos.

This page is intentionally left blank

TABLE OF CONTENTS

ACKNOWLEDGEMENTS I

ABSTRACT III

RESUMO V

TABLE OF CONTENTS VII

LIST OF FIGURES XI

LIST OF TABLES XIII

1 | INTRODUCTION 1

1.1 OVERVIEW 1

1.2 OBJECTIVES 2

2 | PLATE THEORIES 3

2.1 CLASSICAL PLATE THEORY (CLPT) 5

2.1.1 DISPLACEMENTS AND STRAINS 6

2.1.2 MATERIAL LAW 7

2.1.3 LAMINATE CONSTITUTIVE EQUATIONS 8

2.2 FIRST-ORDER SHEAR DEFORMATION THEORY (FSDT) 10

2.2.1 DISPLACEMENTS AND STRAINS 11

2.2.2 MATERIAL LAW 13

2.2.3 LAMINATE CONSTITUTIVE EQUATIONS 14

3 | EXPERIMENTAL PROGRAM 16

3.1 SPECIMEN SPECIFICATION 16

3.1.1 GEOMETRY 16

3.1.2 SPECIFICATIONS FOR CALCULATIONS & TESTS 17

3.2 EXPERIMENTAL PROCEDURE 18

3.3 Experimental Test Set-up 19

4 | BUCKLING OF COMPOSITE PLATES 20

4.1 State of the art 22

4.2 Buckling Analysis 25

4.2.1 Analytical Approach 25

5 | FINITE ELEMENT INVESTIGATIONS 31

5.1 Principles of Finite element method 31

5.2 Finite Element Buckling-Analysis 32

5.2.1 Finite Element Model 33

5.3 Calculations in Ansys: Element Analysis 35

5.3.1 Approach 36

5.3.2 Element Type Definitions 36

5.4 Calculations in Ansys: Mesh Size Comparison 38

6 | ANALYSIS OF RESULTS 39

6.1 Analytical, Numerical and Experimental Buckling Analysis 39

6.1.1 Out-of-plane vs. in-plane displacements 39

6.1.2 Strains resulting from in-plane displacement 41

6.2 Finite Element Analysis 43

6.3 Mesh Size Analysis 45

6.3.1 Mesh size Influence in x-direction for different element types 45

6.3.2 Ansys mesh size Influence in x-direction and z-direction for Solid 45 49

6.4 Discussion of Results 50

6.4.1 Analytical Buckling Analysis 50

6.4.2 Finite Element Buckling Analysis 50

6.4.3 Experimental Results 51

6.4.4 Comparison of Analytical, Numerical and Experimental Results 51

6.4.5 Displacement Shape Comparison 51

6.4.6 Ansys: Element Type Comparison 51

6.4.7 Ansys: Mesh Size Comparison 52

7 | CONCLUSION 53

7.1 CONCLUSION OF RESULTS 53

7.2 LIMITATIONS 55

7.3 FUTURE WORK 55

BIBLIOGRAPHY 56

A | APPENDIX II

A.1 BUCKLING ANALYSIS RESULTS II

A.1.1 OUT-OF-PLANE BUCKLING SHAPE COMPARISON II

A.2 ANSYS ELEMENT ANALYSIS IV

A.3 ANSYS MESH SIZE ANALYSIS VIII

A.3.1 STRAIN COMPARISON OF ELEMENT TYPES VIII

A.3.2 OUT-OF-PLANE DEFLECTION SHAPE COMPARISON XII

This page is intentionally left blank

LIST OF FIGURES

Figure 1: Composite material sailing yacht “Encore” by *Alloy Yachts.* [3] 2
Figure 2: Undeformed and deformed plate for CLPT and FSDT. [5] 4
Figure 3: Undeformed and deformed geometries of an edge of a plate under the assumptions of the Kirchhoff theory. [8] 5
Figure 4: Undeformed and deformed geometries of an edge of a plate under the assumptions of the Mindlin theory. [8] 11
Figure 5: Test specimen geometry without clamped ends. 17
Figure 6: Apparatus and test set-up of the practical experiment. 19
Figure 7: Rectangular plate subjected to in-plane edge loading. [4] 20
Figure 8: Buckling States of Equilibrium. [4] 21
Figure 9: State of Bifurcation. [4] 21
Figure 10: Buckling mode shapes of a clamped-clamped column. [4] 22
Figure 11: Clamped-clamped plate under uni-axial compressive load. [10] 25
Figure 12: First buckling mode shape of a clamped-clamped column. [10] 26
Figure 13: Flow chart load of model in the software of *Ansys*. 32
Figure 14: Applied boundary conditions in form of structural displacements in mm for a clamped-free-clamped-free plate in *Ansys*. 34
Figure 15: Finest calculated mesh geometry of this study. 38
Figure 16: Displacement results for t = 7.92 mm 39
Figure 17: Displacement results for t = 5.31 mm 40
Figure 18: Displacement results for t = 2.49 mm 40
Figure 19: Compressive and tensile strain results for t = 7.92 mm 41
Figure 20: Compressive and tensile strain results for t = 5.31 mm 42
Figure 21: Compressive and tensile strain results for t = 2.49 mm 42
Figure 22: w-deflections for element length of 1 mm in x-direction (t = 5.31 mm). 43
Figure 23: w-deflections for element length of 2 mm in x-direction (t = 5.31 mm). 44
Figure 24: w-deflections for element length of 5 mm in x-direction (t = 5.31 mm). 44
Figure 25: Solid 46 mesh size influence of deflection in x-direction. 45
Figure 26: Solid 45 mesh size influence of deflection in x-direction. 46
Figure 27: Solid 185 mesh size influence of deflection in x-direction. 46
Figure 28: Solid 186 mesh size influence of deflection in x-direction. 47
Figure 29: Solid 95 mesh size influence of deflection in x-direction. 47
Figure 30: Solid 64 mesh size influence of deflection in x-direction. 48
Figure 31: Average mesh size influence of deflection in x-direction. 48

Figure 32: Results of mesh size variation in z-direction (t=5.31 mm, u = 1.5 mm). 49
Figure 33: Results of mesh size variation in x-direction (t = 5.31 mm, u = 1.5 mm). 49
Figure 34: Strains for element corner length of 1 mm in x-direction (t = 5.31 mm). v
Figure 35: Strains for element corner length of 2 mm in x-direction (t = 5.31 mm). v
Figure 36: Strains for element corner length of 5 mm in x-direction (t = 5.31 mm). vi
Figure 37: Solid 46 mesh size influence of strain in x-direction. viii
Figure 38: Solid 45 mesh size influence of strain in x-direction. ix
Figure 39: Solid 185 mesh size influence of strain in x-direction. ix
Figure 40: Solid 186 mesh size influence of strain in x-direction. x
Figure 41: Solid 95 mesh size influence of strain in x-direction. x
Figure 42: Solid 64 mesh size influence of strain in x-direction. xi
Figure 43: Average element mesh size influence of strain in x-direction xi

LIST OF TABLES

Table 1: Lay-up specification of test specimen 17
Table 2: Relative Errors for u = 1.5 mm 41
Table 3: Out-of-plane transverse buckling shapes for t = 7.92 mm ii
Table 4: Out-of-plane transverse buckling shapes for t = 5.31 mm iii
Table 5: Out-of-plane transverse buckling shapes for t = 2.49 mm iii
Table 6: Standard Deviation of w-deflections..... iv
Table 7: Deflection shape for element corner length of 1 mm. vi
Table 8: Deflection shape for element corner length of 2 mm. vii
Table 9: Deflection shape for element corner length of 5 mm. vii
Table 10: Solid 46 w-deflection shape. xii
Table 11: Solid 45 w-deflection shape. xii
Table 12: Solid 185 w-deflection shape. xiii
Table 13: Solid 186 w-deflection shape. xiv
Table 14: Solid 95 w-deflection shape. xiv
Table 15: Solid 64 w-deflection shape. xv
Table 16: Average element w-deflection shape. xv

This page is intentionally left blank

1 | INTRODUCTION

1.1 Overview

Composite materials in plate geometries are used widely throughout various engineering disciplines. Especially the shipbuilding, wind turbine and aerospace industry have strong interest in the advantages of composite materials. Those fibre-reinforced plastics (FRP) are a strongly emerging market with a bright future in lightweight and high performance structures.

Modern Composite Materials consist of two or more identifiable different materials that show other mechanical properties when combined, than independent from each other. Typically, they consist of a matrix and a reinforcement material. The matrix material distributes the loads through the reinforcements and in between them. Further the matrix keeps the reinforcement materials in place. Composites can be of numerous different materials as they can vary in different types of matrix and in different types of reinforcements. [1]

The most important advantage of composite materials is that their anisotropy or properties can be controlled effectively. This means that various mechanical properties can be achieved in different directions within one structural object. In order to do so, variables as fibre volume fraction, fibre direction and amount of layers can be varied. Longitudinal properties of laminates can be controlled by fibre properties, such as material choice and amount of reinforcements. The bond in between different layers in a laminate is generally assumed to be perfect. [2]

This study focuses on unidirectional fibre composite plates to identify mechanical behaviour related to this specific axis. Further, the study handles a profound investigation on the numerical and analytical computation influences.

With a small percentage of exceptions, the marine composite industry is usually defined by a low budget and relatively low requirement for weight reduction, compared with other composite industries as the aerospace for instance. [1]

Marine composite materials are usually polymer matrix composites. More precisely the great majority in the marine industry are (FRP), containing glass fibres (“Glass Reinforced Plastics” - GRP). Depending on budget and application the quality of these GRP vary in form of different fibre materials, order and length of the glass fibres and the type of resin as a matrix. [1]

In this study the focus lies on fibreglass reinforced marine composites, which are most commonly used in the yacht building industry (see table 1, page 17). More precisely the material chosen for this study is e-glass as reinforcement material in woven form and vinylester resin as matrix material. This combination of material is affordable and satisfies the requirements for the majority of the industry in terms of structural ability to weight ratio.

Figure 1: Composite material sailing yacht “Encore” by *Alloy Yachts.* [3]

The matrix material of vinylester brings advantages in form of superior corrosion resistance, better secondary bonding properties, better hydrolytic stability and excellent structural properties like fatigue and impact resistance. Vinylester is more expensive than polyester resin, but cheaper than the high performance epoxy resins. [1]

E-glass fibre reinforcement material is one of the most affordable reinforcement materials in the industry. Its mechanical properties are relatively low compared to the more expensive materials like s-glass or carbon. However, e-glass fibres are satisfying the needs for most applications of the yacht building and marine industry. Only for projects with very high budget and in need of very high performance requirements or weight minimization, the expensive materials of carbon reinforcement fibres and epoxy resin are chosen.

A detailed overview over the most common modern composite materials and their structural abilities can be found in [1].

1.2 Objectives

This study handles a detailed investigation about a specific buckling case of composite plates. The specific buckling case of a clamped-free-clamped-free composite material plate under uniaxial compression loading is investigated in three different ways. Analytical and finite element

analysis (FEA) computations are compared with the results of experimental laboratory tests. The analytical and numerical methods are in themselves investigated. By applying different plate theories to the analytical model and analysing different element types during the finite element calculations, this study presents the differences resulting from these options. In addition to that, this thesis handles an analysis of the influence of different mesh sizes during a finite element analysis.

The aim of this thesis is to compare the analytical, numerical and experimental results of three different marine composite plate thicknesses for the buckling case. Throughout the calculations and experiments, the geometry and boundary conditions are held constant for each of the three plates.
In order to achieve the goal of comparing and analysing the different approaches with each other, the scope of this thesis is distributed as follows:

- First, analytical calculations are done using the software of *Maple.* As well classical laminated plate theory (CLPT), as first-order of shear deformation theory (FSDT) is applied to calculate out-of-plane deflections and maximum longitudinal strains resulting from in-plane deflections, also regarded as end-shortening.
- The second step of this work is to perform a finite element analysis using the software of *Ansys 11*. Therefore, the composite plate is modelled and subjected to uniaxial compressive loading in form of in-plane end-shortening.
- For comparison with realistic values, experimental tests of the previously simulated buckling cases are performed in the laboratory and documented precisely.
- A comparison of different element types and mesh refinements of the group of structural 3D elements in *Ansys 11* is done.
- Results are documented and compared with each other, as far as reasonable.
- Finally, conclusions are stated based on the results of each chapter.

2 | PLATE THEORIES

Plates are defined as a structural element with plan form dimension that are large compared to its thickness. When uniaxial in-plane loads are applied to plates, it causes in-plane compression that is followed by a sudden lateral deflection of the plate when the load overcomes the critical buckling load. Because of its small thickness to in-plane dimension ratio is usually sufficient to

apply a 2D instead of a 3D model to the elasticity deformation relations. The two most relevant single layer theories (2D), which are applied in this study, are the following:

- Classical Plate Theory (CLPT)
- First-Order Shear Deformation Theory (FSDT)

The CLPT theory is the simpler one of the two investigated. The theory was developed by Gustav R. Kirchhoff and is an extension of the Euler-Bernoulli Beam theory to composite laminated plates. [4]
Based on the hypothesis of Reissner and Mindlin the theory of FSDT was developed. This theory is based on the CLPT theory and extended by removing the restriction that the transverse normals remain perpendicular to the mid-surface after deformation. A comparison of the two theories is graphically shown in figure 2.

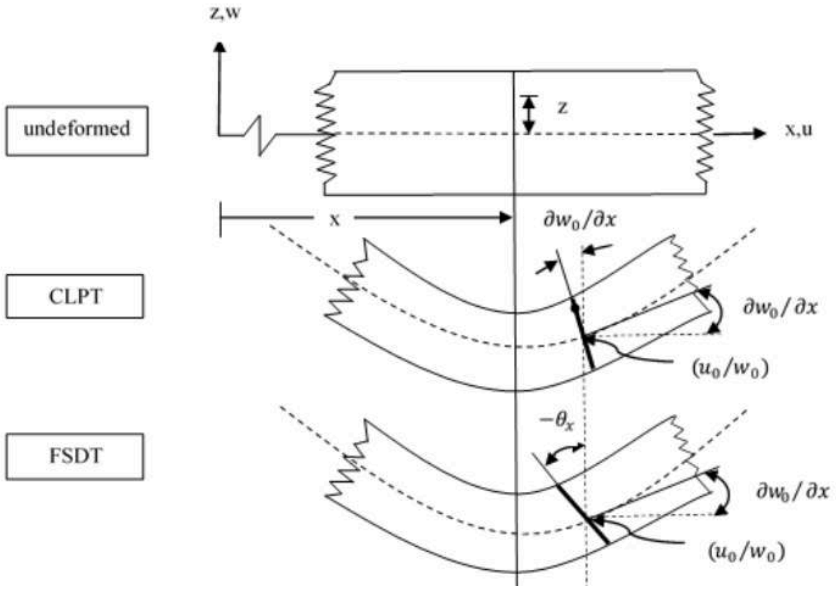

Figure 2: Undeformed and deformed plate for CLPT and FSDT. [5]

The laminated plates are made out of plies, while each ply consists many parallel reinforcement fibres embedded in a matrix material. These special structural properties need to be taken into account in the calculations. Mathematical models discretize these aspects by considering the neutral axis and fibre direction of each ply. [6]

2.1 Classical Plate Theory (CLPT)

The CLPT developed by Gustav R. Kirchhoff in 1850 is often also referred to as thin plate theory. The reason for this is that the theory is mostly suitable for thin plates or shell-like structures. This theory implies that the hypothesis of Kirchhoff holds, which consists of the following three parts.[6]

- Straight lines perpendicular to the mid-surface of the flat plate remain perpendicular to the mid-surface after deformation.
- The thickness of the plate is constant throughout the bending process.
- The transverse normals to the mid-surface rotate in a way that they stay perpendicular to the mid-surface after deformation.

These assumptions imply that the classical plate theory neglects transverse normals and shear stresses. This leads to a slight underestimation of buckling loads and deflection.

Figure 3 shows the undeformed and deformed geometry of an edge of a plate under the assumption of the Kirchhoff hypothesis.

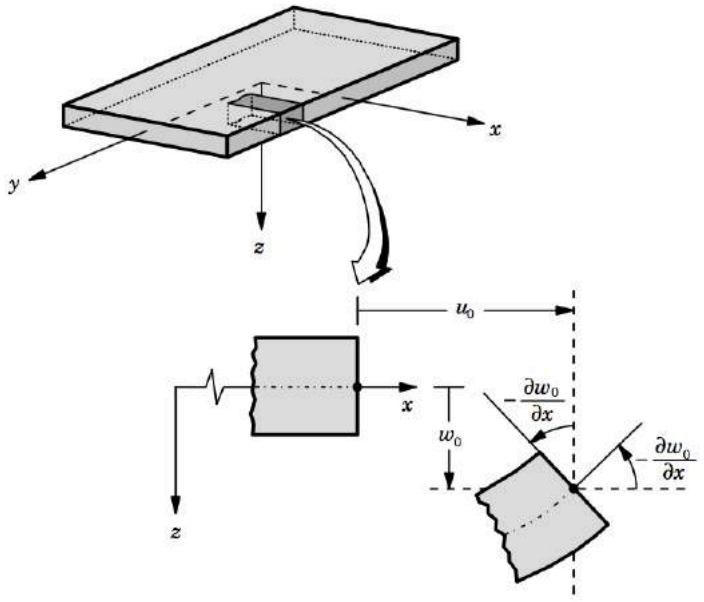

Figure 3: Undeformed and deformed geometries of an edge of a plate under the assumptions of the Kirchhoff theory. [8]

2.1.1 Displacements and Strains

The kinematic relation of displacements is expressed by the following set of equations (2.1 - 2.3).

$$u(x,y,z) = u_0(\mathrm{x},\mathrm{y}) - \mathrm{z}\frac{\partial \mathrm{w}}{\partial \mathrm{x}} \tag{2.1}$$

$$v(x,y,z) = v_0(x,y) - \mathrm{z}\frac{\partial \mathrm{w}}{\partial \mathrm{y}} \tag{2.2}$$

$$w(x,y,z) = w_0(x,y) \tag{2.3}$$

where, u, v and z are the displacement components in x, y and direction respectively and $u_{0,}\, v_{0,}\, z_0$ the displacements of the mid-surface in x, y and z direction respectively. [8]

The strain-displacement relation including linear and non-linear strains are described by the following expression [9]:

$$\{\varepsilon\} = \begin{Bmatrix} \varepsilon_x \\ \varepsilon_y \\ \gamma_{xy} \end{Bmatrix} = \begin{Bmatrix} \varepsilon_{l,x} \\ \varepsilon_{l,y} \\ \gamma_{l,xy} \end{Bmatrix} + \begin{Bmatrix} \varepsilon_{nl,x} \\ \varepsilon_{nl,y} \\ \gamma_{nl,xy} \end{Bmatrix} + z \begin{Bmatrix} \psi_{,x} \\ \psi_y \\ \psi_{xy} \end{Bmatrix} \tag{2.4}$$

where $\varepsilon_x \text{ and } \varepsilon_y$ are the in-plane normal strains and γ_{xy} the in-plane shear strain.

The linear strain-displacement relation of classical plane elasticity theory is [9]:

$$\{\varepsilon_l\} = \begin{Bmatrix} \varepsilon_{l,x} \\ \varepsilon_{l,y} \\ \gamma_{l,xy} \end{Bmatrix} = \begin{Bmatrix} \dfrac{\partial \mathrm{u}_0}{\partial \mathrm{x}} \\ \dfrac{\partial \mathrm{v}_0}{\partial \mathrm{y}} \\ \dfrac{\partial \mathrm{u}_0}{\partial \mathrm{y}} + \dfrac{\partial \mathrm{v}_0}{\partial \mathrm{x}} \end{Bmatrix} \tag{2.5}$$

where $\varepsilon_{l,x}, \varepsilon_{l,y}$ and $\gamma_{l,xy}$ are the mid-plane strains.

The non-linear strain-displacement relation is [9]:

$$\{\varepsilon_{nl}\} = \begin{Bmatrix} \varepsilon_{nl,x} \\ \varepsilon_{nl,y} \\ \gamma_{nl,xy} \end{Bmatrix} = \begin{Bmatrix} \dfrac{1}{2}\left(\dfrac{\partial \mathrm{w}_0}{\partial \mathrm{x}}\right)^2 \\ \dfrac{1}{2}\left(\dfrac{\partial \mathrm{u}}{\partial \mathrm{y}}\right)^2 \\ \dfrac{\partial \mathrm{w}_0}{\partial \mathrm{x}} + \dfrac{\partial \mathrm{w}_0}{\partial \mathrm{y}} \end{Bmatrix} \tag{2.6}$$

where $\varepsilon_{nl,x}, \varepsilon_{nl,y}$ and $\gamma_{nl,xy}$ are the non-linear strains which allow for large displacements.

The bending strain-displacement relation is [9]:

$$\{\psi\} = \begin{Bmatrix} \psi_{,x} \\ \psi_y \\ \psi_{xy} \end{Bmatrix} = \begin{Bmatrix} -\frac{\partial^2 \mathrm{w}_0}{\partial \mathrm{x}^2} \\ -\frac{\partial^2 \mathrm{u}_0}{\partial \mathrm{y}^2} \\ -2\frac{\partial^2 \mathrm{w}_0}{\partial \mathrm{y}\,\partial \mathrm{x}} \end{Bmatrix} \tag{2.7}$$

where $\psi_{,x}, \psi_{,y}$ and $\psi_{,xy}$ are the curvature changes of the mid-plane during deformations.

This eventually leads to the strain expression in form of displacement as follows [9]:

$$\{\varepsilon\} = \begin{Bmatrix} \varepsilon_x \\ \varepsilon_y \\ \gamma_{xy} \end{Bmatrix} = \begin{Bmatrix} \frac{\partial}{\partial \mathrm{x}} u_0 \\ \frac{\partial}{\partial \mathrm{y}} v_0 \\ \frac{\partial}{\partial \mathrm{y}} u_0 \end{Bmatrix} + \begin{Bmatrix} \frac{1}{2}\left(\frac{\partial \mathrm{w}_0}{\partial \mathrm{x}}\right)^2 \\ \frac{1}{2}\left(\frac{\partial \mathrm{u}}{\partial \mathrm{y}}\right)^2 \\ \frac{\partial \mathrm{w}_0}{\partial \mathrm{x}}\frac{\partial \mathrm{w}_0}{\partial \mathrm{y}} \end{Bmatrix} + z \begin{Bmatrix} -\frac{\partial^2 w_0}{\partial x^2} \\ -\frac{\partial^2 w_0}{\partial x^2} \\ -2\frac{\partial^2 w_0}{\partial \mathrm{x}\,\partial \mathrm{x}} \end{Bmatrix} \tag{2.8}$$

2.1.2 Material Law

The stress-strain relation is given as follows [10]:

$$\begin{Bmatrix} \sigma_x \\ \sigma_y \\ \tau_{xy} \end{Bmatrix} = [\bar{Q}] \begin{Bmatrix} \varepsilon_x \\ \varepsilon_y \\ \gamma_{xy} \end{Bmatrix} = \begin{bmatrix} \bar{Q}_{11} & \bar{Q}_{12} & \bar{Q}_{16} \\ \bar{Q}_{12} & \bar{Q}_{22} & \bar{Q}_{26} \\ \bar{Q}_{16} & \bar{Q}_{26} & \bar{Q}_{66} \end{bmatrix} \begin{Bmatrix} \varepsilon_x \\ \varepsilon_y \\ \gamma_{xy} \end{Bmatrix} \tag{2.9}$$

where [11]:

$$\bar{Q}_{11} = Q_{11}cos^4\theta + 2(Q_{12} + Q_{66})sin^2\theta cos^2\theta + Q_{66}sin^4\theta \tag{2.10}$$

$$\bar{Q}_{12} = (Q_{11} + Q_{22} - 4Q_{66})sin^2\theta cos^2\theta + Q_{66}(sin^4\theta + cos^4\theta) \tag{2.11}$$

$$\bar{Q}_{16} = (Q_{11} - Q_{22} - 2Q_{66})sin\theta cos^3\theta + (Q_{11} - Q_{22} + 2Q_{66})sin^3\theta cos\theta \tag{2.12}$$

$$\bar{Q}_{22} = Q_{11}sin^4\theta + 2(Q_{12} + Q_{66})sin^2\theta cos^2\theta + Q_{66}cos^4\theta \tag{2.13}$$

$$\bar{Q}_{26} = (Q_{11} - Q_{22} - 2Q_{66})cos\theta sin^3\theta + (Q_{11} - Q_{22} + 2Q_{66})cos^3\theta sin\theta \tag{2.14}$$

$$\bar{Q}_{66} = (Q_{11} + Q_{22} - 2Q_{12} - 2Q_{66})sin^2\theta cos^2\theta + Q_{66}(sin^4\theta + cos^4\theta) \tag{2.15}$$

where θ is the lay-up angle of reinforcement.

and [10]

$$Q_{11} = \frac{E_1}{1 - v_{12}v_{21}};\ Q_{12} = \frac{v_{12}E_2}{1 - v_{12}v_{21}};\ Q_{22} = \frac{E_2}{1 - v_{12}v_{21}};\ Q_{66} = Q_{12}; \tag{2.16}$$

hence [10]

$$\begin{Bmatrix} \sigma_x \\ \sigma_y \\ \tau_{xy} \end{Bmatrix} = \begin{bmatrix} \bar{Q}_{11} & \bar{Q}_{12} & \bar{Q}_{16} \\ \bar{Q}_{12} & \bar{Q}_{22} & \bar{Q}_{26} \\ \bar{Q}_{16} & \bar{Q}_{26} & \bar{Q}_{66} \end{bmatrix} \begin{Bmatrix} \varepsilon_{l,x} & \varepsilon_{nl,x} \\ \varepsilon_{l,y} & + \varepsilon_{nl,y} \\ \gamma_{l,xy} & \gamma_{nl,y} \end{Bmatrix} + z \begin{bmatrix} \bar{Q}_{11} & \bar{Q}_{12} & \bar{Q}_{16} \\ \bar{Q}_{12} & \bar{Q}_{22} & \bar{Q}_{26} \\ \bar{Q}_{16} & \bar{Q}_{26} & \bar{Q}_{66} \end{bmatrix} \begin{Bmatrix} \psi_{,x} \\ \psi_y \\ \psi_{xy} \end{Bmatrix} \tag{2.17}$$

2.1.3 Laminate Constitutive Equations

Here, the relations between forces and moment resultants and strains are derived. We neglect the effects of temperature and piezoelectricity. Further, we assume that each layer obeys Hooke's Law and that each ply is orthogonal with its symmetry lines.

Since stresses throughout the laminate vary with each layer, it is convenient to simplify the system of layers to an equivalent system by integrating the corresponding stresses over the laminate thickness.

In general form the membrane direct and shearing stress resultants per unit length N_x, N_y and N_{xy} and the bending and twisting stress couples per unit length M_x, M_y and M_{xy} are related to the in- and out-of-plane displacements as follows [11].

$$\begin{Bmatrix} \mathrm{N}_x \\ \mathrm{N}_y \\ \mathrm{N}_{xy} \\ \mathrm{M}_x \\ \mathrm{M}_y \\ \mathrm{M}_{xy} \end{Bmatrix} = \int_{-\frac{t}{2}}^{\frac{t}{2}} \begin{Bmatrix} \sigma_x \\ \sigma_y \\ \tau_{xy} \\ z\sigma_x \\ z\sigma_y \\ z\tau_{xy} \end{Bmatrix} dz = \begin{bmatrix} [A] & [B] \\ [B] & [D] \end{bmatrix} \begin{Bmatrix} \{\varepsilon_l\} + \{\varepsilon_{nl}\} \\ \{\psi\} \end{Bmatrix} \tag{2.18}$$

where [12]

$$[A_{mn}], [B_{mn}], [D_{mn}] = \int_{\frac{t}{2}}^{\frac{t}{2}} [\overline{Q_{mn}}]\,(1, z, z^2)dz\,; m, n = 1,2,6 \tag{2.19}$$

This leads to the following normal force resultants with respect to the coordinate system [10].

$$\begin{Bmatrix} N_x \\ N_y \\ N_{xy} \end{Bmatrix} = \int_{\frac{-h}{2}}^{\frac{h}{2}} \begin{Bmatrix} \sigma_x \\ \sigma_y \\ \tau_{xy} \end{Bmatrix} dz = \sum_{i=1}^{n} \int_{hi-1}^{hi} \begin{Bmatrix} \sigma_x \\ \sigma_y \\ \tau_{xy} \end{Bmatrix} dz \tag{2.20}$$

Integrating the stresses multiplied with the lever arm to the mid-surface leads to the moment [10].

$$\begin{Bmatrix} M_x \\ M_y \\ M_{xy} \end{Bmatrix} = \int_{\frac{-h}{2}}^{\frac{h}{2}} \begin{Bmatrix} \sigma_x \\ \sigma_y \\ \tau_{xy} \end{Bmatrix} z dz = \sum_{i=1}^{n} \int_{hi-1}^{hi} \begin{Bmatrix} \sigma_x \\ \sigma_y \\ \tau_{xy} \end{Bmatrix} dz \tag{2.21}$$

The resulting normal forces are thus [10]:

$$\begin{aligned} \begin{Bmatrix} N_x \\ N_y \\ N_{xy} \end{Bmatrix} = & \sum_{i=1}^{n} \int_{\frac{-h}{2}}^{\frac{h}{2}} \begin{bmatrix} \bar{Q}_{11} & \bar{Q}_{12} & \bar{Q}_{16} \\ \bar{Q}_{12} & \bar{Q}_{22} & \bar{Q}_{26} \\ \bar{Q}_{16} & \bar{Q}_{26} & \bar{Q}_{66} \end{bmatrix} dz \begin{Bmatrix} \varepsilon_{l,x} & \varepsilon_{nl,x} \\ \varepsilon_{l,y} & + \varepsilon_{nl,y} \\ \gamma_{l,xy} & \gamma_{nl,xy} \end{Bmatrix} \\ & + \sum_{i=1}^{n} \int_{\frac{-h}{2}}^{\frac{h}{2}} \begin{bmatrix} \bar{Q}_{11} & \bar{Q}_{12} & \bar{Q}_{16} \\ \bar{Q}_{12} & \bar{Q}_{22} & \bar{Q}_{26} \\ \bar{Q}_{16} & \bar{Q}_{26} & \bar{Q}_{66} \end{bmatrix} dz \begin{Bmatrix} \psi_{,x} \\ \psi_y \\ \psi_{xy} \end{Bmatrix} \end{aligned} \tag{2.22}$$

hence [10]

$$\begin{aligned} \begin{Bmatrix} N_x \\ N_y \\ N_{xy} \end{Bmatrix} = & \begin{bmatrix} A_{11} & A_{12} & A_{16} \\ A_{12} & A_{22} & A_{26} \\ A_{16} & A_{26} & A_{66} \end{bmatrix} \begin{Bmatrix} \frac{\partial}{\partial \mathrm{x}} u_0 + \frac{1}{2} \left(\frac{\partial \mathrm{w}_0}{\partial \mathrm{x}} \right)^2 \\ \frac{\partial}{\partial \mathrm{y}} v_0 + \frac{1}{2} \left(\frac{\partial \mathrm{u}}{\partial \mathrm{y}} \right)^2 \\ \frac{\partial}{\partial \mathrm{y}} u_0 + \frac{\partial}{\partial \mathrm{x}} v_0 + \frac{\partial \mathrm{w}_0}{\partial \mathrm{x}} \frac{\partial \mathrm{w}_0}{\partial \mathrm{y}} \end{Bmatrix} \\ & + \begin{bmatrix} B_{11} & B_{12} & B_{16} \\ B_{12} & B_{22} & B_{26} \\ B_{16} & B_{26} & B_{66} \end{bmatrix} \begin{Bmatrix} -\frac{\partial^2}{\partial x^2} w_0 \\ -\frac{\partial^2}{\partial x^2} w_0 \\ -2 \frac{\partial^2}{\partial \mathrm{x} \, \partial \mathrm{x}} w_0 \end{Bmatrix} \end{aligned} \tag{2.23}$$

The resulting bending moments are thus [10]:

$$\begin{aligned} \begin{Bmatrix} M_x \\ M_y \\ M_{xy} \end{Bmatrix} = & \sum_{i=1}^{n} \int_{\frac{-h}{2}}^{\frac{h}{2}} z \begin{bmatrix} \bar{Q}_{11} & \bar{Q}_{12} & \bar{Q}_{16} \\ \bar{Q}_{12} & \bar{Q}_{22} & \bar{Q}_{26} \\ \bar{Q}_{16} & \bar{Q}_{26} & \bar{Q}_{66} \end{bmatrix} dz \begin{Bmatrix} \varepsilon_{l,x} & \varepsilon_{nl,x} \\ \varepsilon_{l,y} & + \varepsilon_{nl,y} \\ \gamma_{l,xy} & \gamma_{nl,xy} \end{Bmatrix} \\ & + \sum_{i=1}^{n} \int_{\frac{-h}{2}}^{\frac{h}{2}} z^2 \begin{bmatrix} \bar{Q}_{11} & \bar{Q}_{12} & \bar{Q}_{16} \\ \bar{Q}_{12} & \bar{Q}_{22} & \bar{Q}_{26} \\ \bar{Q}_{16} & \bar{Q}_{26} & \bar{Q}_{66} \end{bmatrix} dz \begin{Bmatrix} \psi_{,x} \\ \psi_y \\ \psi_{xy} \end{Bmatrix} \end{aligned} \tag{2.24}$$

hence [10]

$$\begin{Bmatrix} M_x \\ M_y \\ M_{xy} \end{Bmatrix} = \begin{bmatrix} B_{11} & B_{12} & B_{16} \\ B_{12} & B_{22} & B_{26} \\ B_{16} & B_{26} & B_{66} \end{bmatrix} \begin{Bmatrix} \frac{\partial}{\partial \mathrm{x}} u_0 + \frac{1}{2}\left(\frac{\partial \mathrm{w}_0}{\partial \mathrm{x}}\right)^2 \\ \frac{\partial}{\partial \mathrm{y}} v_0 + \frac{1}{2}\left(\frac{\partial \mathrm{u}}{\partial \mathrm{y}}\right)^2 \\ \frac{\partial}{\partial \mathrm{y}} u_0 + \frac{\partial}{\partial \mathrm{x}} v_0 + \frac{\partial \mathrm{w}_0}{\partial \mathrm{x}} \frac{\partial \mathrm{w}_0}{\partial \mathrm{y}} \end{Bmatrix} + \begin{bmatrix} D_{11} & D_{12} & D_{16} \\ D_{12} & D_{22} & D_{26} \\ D_{16} & D_{26} & D_{66} \end{bmatrix} \begin{Bmatrix} -\frac{\partial^2}{\partial x^2} w_0 \\ -\frac{\partial^2}{\partial x^2} w_0 \\ -2\frac{\partial^2}{\partial \mathrm{x}\, \partial \mathrm{x}} w_0 \end{Bmatrix} \tag{2.25}$$

2.2 First-Order Shear Deformation Theory (FSDT)

The FSDT developed by Reissner and Mindlin in 1951 relaxes the normality restrictions of the CLPT and therefore extends the kinematics. This means, that in FSDT arbitrary rotations of the transverse normals to the mid-plane are considered. Since the theory takes shear forces into account, it is more accurate than the classical theory. Depending on the relative plate thickness, the buckling load or deformations of the applied FSDT theory will always be higher than from of CLPT.

Thus, the theory is based on the following assumptions [8]:

- Straight lines perpendicular to the mid-surface of the flat plate remain perpendicular to the mid-surface after deformation.
- The thickness of the plate is constant throughout the bending process.

FSDT includes a gross transverse shear deformation in its kinematic assumptions. Shear strains are assumed to be constant with the distance from the mid-surface. The theory requires a shear correction factors (k). This factor depends on lamination and geometric parameters and also on the loading and boundary conditions. It is chosen to be $k = 0.83$. [8]
The shear correction factor k handles the discrepancy between the actual stress state and the, from the first-order shear theory predicted, constant stress state by multiplying the integrals in the shear force resultants calculation with a parameter k. [4]

2.2.1 Displacements and Strains

The relation between in-plane and normal displacements is represented by the following set of equations (2.26 – 2.28). [8]

$$u(x,y,z) = u_0(\mathrm{x},\mathrm{y}) + \mathrm{z}\phi_x(x,y) \tag{2.26}$$

$$v(x,y,z,t) = v_0(\mathrm{x},\mathrm{y}) + \mathrm{z}\phi_y(x,y) \tag{2.27}$$

$$w(x,y,z) = w_0(x,y) \tag{2.28}$$

where u, v and z are the displacement components in x, y and z direction respectively, $u_0, v_0, \text{and } z_0$ the displacements of the mid-surface in x, y and z direction respectively and ϕ_x, ϕ_y rotations about the transverse normal about the x and y-axis respectively as shown in figure 4.

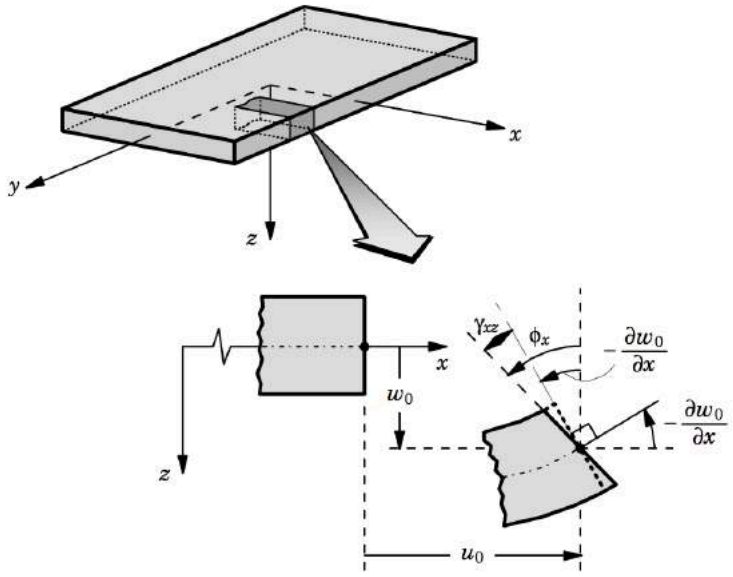

Figure 4: Undeformed and deformed geometries of an edge of a plate under the assumptions of the Mindlin theory. [8]

In the FSDT the strain vector implies the Green-Lagrange strain vector components in terms of the displacements with the non-linear strains included in the Von-Karman sense. [9]

The strains depending on mid-plane displacements can be written as follows [12]:

$$\begin{Bmatrix} \varepsilon \\ \gamma \end{Bmatrix} = \begin{Bmatrix} \varepsilon_{p,l} \\ 0 \end{Bmatrix} + \begin{Bmatrix} \varepsilon_{p,nl} \\ 0 \end{Bmatrix} + \begin{Bmatrix} z\varepsilon_b \\ \gamma \end{Bmatrix} \tag{2.29}$$

The linear strain-displacement relation is [11]:

$$\{\varepsilon_l\} = \begin{Bmatrix} \varepsilon_{l,x} \\ \varepsilon_{l,y} \\ \gamma_{l,xy} \end{Bmatrix} = \begin{Bmatrix} \dfrac{\partial \mathrm{u}_0}{\partial \mathrm{x}} \\ \dfrac{\partial \mathrm{v}_0}{\partial \mathrm{y}} \\ \dfrac{\partial \mathrm{u}_0}{\partial \mathrm{y}} + \dfrac{\partial \mathrm{v}_0}{\partial \mathrm{x}} \end{Bmatrix} \tag{2.30}$$

The non-linear strain-displacement relation is [11]:

$$\{\varepsilon_{nl}\} = \begin{Bmatrix} \varepsilon_{nl,x} \\ \varepsilon_{nl,y} \\ \gamma_{nl,xy} \end{Bmatrix} = \begin{Bmatrix} \dfrac{1}{2}\left(\dfrac{\partial \mathrm{w}_0}{\partial \mathrm{x}}\right)^2 \\ \dfrac{1}{2}\left(\dfrac{\partial \mathrm{u}}{\partial \mathrm{y}}\right)^2 \\ \dfrac{\partial \mathrm{w}_0}{\partial \mathrm{x}} \dfrac{\partial \mathrm{w}_0}{\partial \mathrm{y}} \end{Bmatrix} \tag{2.31}$$

The bending strain-displacement relation is [11]:

$$\{\psi\} = \begin{Bmatrix} \psi_{,x} \\ \psi_y \\ \psi_{xy} \end{Bmatrix} = \begin{Bmatrix} \frac{\partial \phi_x}{\partial \mathrm{x}} \\ \frac{\partial \phi_y}{\partial \mathrm{y}} \\ \frac{\partial \phi_x}{\partial \mathrm{y}} + \frac{\partial \phi_y}{\partial \mathrm{x}} \end{Bmatrix} \tag{2.32}$$

The shear strain-displacement relation is [11]:

$$\{\gamma\} = \begin{Bmatrix} \gamma_{yz} \\ \gamma_{xz} \end{Bmatrix} = \begin{Bmatrix} \phi_y + \dfrac{\partial \mathrm{w}_0}{\partial \mathrm{y}} \\ \phi_x + \dfrac{\partial \mathrm{w}_0}{\partial \mathrm{x}} \end{Bmatrix} \tag{2.33}$$

This eventually leads to:

$$\{\varepsilon\} = \begin{Bmatrix} \varepsilon_x \\ \varepsilon_y \\ \gamma_{xy} \end{Bmatrix} = \begin{Bmatrix} \dfrac{\partial \mathrm{u}_0}{\partial \mathrm{x}} \\ \dfrac{\partial \mathrm{v}_0}{\partial \mathrm{y}} \\ \dfrac{\partial \mathrm{u}_0}{\partial \mathrm{y}} + \dfrac{\partial \mathrm{v}_0}{\partial \mathrm{x}} \end{Bmatrix} + \begin{Bmatrix} \dfrac{1}{2}\left(\dfrac{\partial \mathrm{w}_0}{\partial \mathrm{x}}\right)^2 \\ \dfrac{1}{2}\left(\dfrac{\partial \mathrm{u}}{\partial \mathrm{y}}\right)^2 \\ \dfrac{\partial \mathrm{w}_0}{\partial \mathrm{x}} \dfrac{\partial \mathrm{w}_0}{\partial \mathrm{y}} \end{Bmatrix} + z \begin{Bmatrix} \dfrac{\partial \phi_x}{\partial \mathrm{x}} \\ \dfrac{\partial \phi_y}{\partial \mathrm{y}} \\ \dfrac{\partial \phi_x}{\partial \mathrm{y}} + \dfrac{\partial \phi_y}{\partial \mathrm{x}} \end{Bmatrix} \tag{2.33}$$

and

$$\{\gamma\} = \begin{Bmatrix}\gamma_{yz}\\ \gamma_{xz}\end{Bmatrix} = \begin{Bmatrix}\phi_y + \frac{\partial w_0}{\partial y}\\ \phi_x + \frac{\partial w_0}{\partial x}\end{Bmatrix} \tag{2.34}$$

2.2.2 Material Law

The stress-strain relation is given as follows [9]:

$$\begin{Bmatrix}\sigma_x\\ \sigma_y\\ \tau_{xz}\\ \tau_{yz}\\ \tau_{xy}\end{Bmatrix} = [\bar{Q}]\begin{Bmatrix}\varepsilon_x\\ \varepsilon_y\\ \gamma_{xz}\\ \gamma_{yz}\\ \gamma_{xy}\end{Bmatrix} = \begin{bmatrix}\bar{Q}_{11} & \bar{Q}_{12} & 0 & 0 & \bar{Q}_{16}\\ \bar{Q}_{12} & \bar{Q}_{22} & 0 & 0 & \bar{Q}_{26}\\ 0 & 0 & \bar{Q}_{44} & 0 & 0\\ 0 & 0 & 0 & \bar{Q}_{55} & 0\\ \bar{Q}_{16} & \bar{Q}_{26} & 0 & 0 & \bar{Q}_{66}\end{bmatrix}\begin{Bmatrix}\varepsilon_x\\ \varepsilon_y\\ \gamma_{xz}\\ \gamma_{yz}\\ \gamma_{xy}\end{Bmatrix} \tag{2.35}$$

where [11]

$$\bar{Q}_{11} = Q_{11}cos^4\theta + 2(Q_{12} + Q_{66})sin^2\theta cos^2\theta + Q_{66}sin^4\theta \tag{2.36}$$

$$\bar{Q}_{12} = (Q_{11} + Q_{22} - 4Q_{66})sin^2\theta cos^2\theta + Q_{66}(sin^4\theta + cos^4\theta) \tag{2.37}$$

$$\bar{Q}_{16} = (Q_{11} - Q_{22} - 2Q_{66})sin\theta cos^3\theta + (Q_{11} - Q_{22} + 2Q_{66})sin^3\theta cos\theta \tag{2.38}$$

$$\bar{Q}_{22} = Q_{11}sin^4\theta + 2(Q_{12} + Q_{66})sin^2\theta cos^2\theta + Q_{66}cos^4\theta \tag{2.39}$$

$$\bar{Q}_{26} = (Q_{11} - Q_{22} - 2Q_{66})cos\theta sin^3\theta + (Q_{11} - Q_{22} + 2Q_{66})cos^3\theta sin\theta \tag{2.40}$$

$$\bar{Q}_{66} = (Q_{11} + Q_{22} - 2Q_{12} - 2Q_{66})sin^2\theta cos^2\theta + Q_{66}(sin^4\theta + cos^4\theta) \tag{2.41}$$

where θ is the lay-up angle of reinforcement

and [10]

$$Q_{11} = \frac{E_1}{1 - v_{12}v_{21}};\ Q_{12} = \frac{v_{12}E_2}{1 - v_{12}v_{21}};\ Q_{22} = \frac{E_2}{1 - v_{12}v_{21}};\ Q_{66} = Q_{12} \tag{2.42}$$

This leads to the following stress-strain relation, while splitting it up into two parts, bending and shear.

Bending stress-strain relation [10]:

$$\begin{Bmatrix}\sigma_x\\ \sigma_y\\ \tau_{xy}\end{Bmatrix}=\begin{bmatrix}\bar{Q}_{11} & \bar{Q}_{12} & \bar{Q}_{16}\\ \bar{Q}_{12} & \bar{Q}_{22} & \bar{Q}_{26}\\ \bar{Q}_{16} & \bar{Q}_{26} & \bar{Q}_{66}\end{bmatrix}\begin{Bmatrix}\frac{\partial}{\partial \mathrm{x}}u_0\\ \frac{\partial}{\partial \mathrm{y}}v_0\\ \frac{\partial}{\partial \mathrm{y}}u_0+\frac{\partial}{\partial \mathrm{x}}v_0\end{Bmatrix}+z\begin{bmatrix}\bar{Q}_{11} & \bar{Q}_{12} & \bar{Q}_{16}\\ \bar{Q}_{12} & \bar{Q}_{22} & \bar{Q}_{26}\\ \bar{Q}_{16} & \bar{Q}_{26} & \bar{Q}_{66}\end{bmatrix}\begin{Bmatrix}\frac{\partial \phi_x}{\partial \mathrm{x}}\\ \frac{\partial \phi_y}{\partial \mathrm{y}}\\ \frac{\partial \phi_x}{\partial \mathrm{y}}+\frac{\partial \phi_y}{\partial \mathrm{x}}\end{Bmatrix} \quad (2.43)$$

Shear stress-strain relation [10]:

$$\begin{Bmatrix}\tau_{yz}\\ \tau_{xz}\end{Bmatrix}=k\begin{bmatrix}\bar{Q}_{44} & \bar{Q}_{45}\\ \bar{Q}_{45} & \bar{Q}_{55}\end{bmatrix}\begin{Bmatrix}\gamma_{yz}\\ \gamma_{xz}\end{Bmatrix}=k\begin{bmatrix}\bar{Q}_{44} & \bar{Q}_{45}\\ \bar{Q}_{45} & \bar{Q}_{55}\end{bmatrix}\begin{Bmatrix}\phi_y+\frac{\partial \mathrm{w}_0}{\partial \mathrm{y}}\\ \phi_x+\frac{\partial \mathrm{w}_0}{\partial \mathrm{x}}\end{Bmatrix} \quad (2.44)$$

where k is the shear correction factor.

2.2.3 Laminate Constitutive Equations

In general form, the membrane direct and shearing stress resultants per unit length N_x, N_y and N_{xy}, the out-of-plane shearing stress resultants Q_x and Q_y per unit length and the bending and twisting stress couples per unit length M_x, M_y and M_{xy} are related to the in- and out-of-plane displacements as follows. [10], [11]

$$\begin{Bmatrix}\mathrm{N}_x\\ \mathrm{N}_y\\ \mathrm{N}_{xy}\\ \mathrm{M}_x\\ \mathrm{M}_y\\ \mathrm{M}_{xy}\\ \mathrm{Q}_x\\ \mathrm{Q}_y\end{Bmatrix}=\int_{-\frac{t}{2}}^{\frac{t}{2}}\begin{Bmatrix}\sigma_x\\ \sigma_y\\ \tau_{xy}\\ z\sigma_x\\ z\sigma_y\\ z\tau_{xy}\\ \tau_{xz}\\ \tau_{yz}\end{Bmatrix}dz=\begin{bmatrix}[A] & [B] & 0\\ [B] & [D] & 0\\ 0 & 0 & [A_s]\end{bmatrix}\begin{Bmatrix}\{\varepsilon_l\}+\{\varepsilon_{nl}\}\\ \{\psi\}\\ \gamma\end{Bmatrix} \quad (2.45)$$

where [11]

$$[A_{mn}],[B_{mn}],[D_{mn}]=\int_{-\frac{t}{2}}^{\frac{t}{2}}[\overline{Q_{mn}}]\,(1,z,z^2)dz \quad ;m,n=1,2,6 \quad (2.46)$$

and [11]

$$[As_{mn}] = \mathrm{k} \int_{\frac{t}{2}}^{\frac{t}{2}} [\overline{Q_{mn}}]\, dz \quad ; m = 4{,}5 \tag{2.47}$$

where k is the shear correction factor.

Following the same calculations as for CLPT to calculate the normal force, shear force and bending moment resultants can be expressed in terms of mid-plane displacements ($u_0,\ v_0,\ w_0$) by the following relations.

The resulting normal forces are thus [10]:

$$\begin{Bmatrix} N_x \\ N_y \\ N_{xy} \end{Bmatrix} = \begin{bmatrix} A_{11} & A_{12} & A_{16} \\ A_{12} & A_{22} & A_{26} \\ A_{16} & A_{26} & A_{66} \end{bmatrix} \begin{Bmatrix} \frac{\partial}{\partial \mathrm{x}} u_0 \\ \frac{\partial}{\partial \mathrm{y}} v_0 \\ \frac{\partial}{\partial \mathrm{y}} u_0 + \frac{\partial}{\partial \mathrm{x}} v_0 \end{Bmatrix} + \begin{bmatrix} B_{11} & B_{12} & B_{16} \\ B_{12} & B_{22} & B_{26} \\ B_{16} & B_{26} & B_{66} \end{bmatrix} \begin{Bmatrix} \frac{\partial \phi_x}{\partial \mathrm{x}} \\ \frac{\partial \phi_y}{\partial \mathrm{y}} \\ \frac{\partial \phi_x}{\partial \mathrm{y}} + \frac{\partial \phi_y}{\partial \mathrm{x}} \end{Bmatrix} \tag{2.48}$$

The resulting bending moments are thus [10]:

$$\begin{Bmatrix} M_x \\ M_y \\ M_{xy} \end{Bmatrix} = \begin{bmatrix} B_{11} & B_{12} & B_{16} \\ B_{12} & B_{22} & B_{26} \\ B_{16} & B_{26} & B_{66} \end{bmatrix} \begin{Bmatrix} \frac{\partial}{\partial \mathrm{x}} u_0 \\ \frac{\partial}{\partial \mathrm{y}} v_0 \\ \frac{\partial}{\partial \mathrm{y}} u_0 + \frac{\partial}{\partial \mathrm{x}} v_0 \end{Bmatrix} + \begin{bmatrix} D_{11} & D_{12} & D_{16} \\ D_{12} & D_{22} & D_{26} \\ D_{16} & D_{26} & D_{66} \end{bmatrix} \begin{Bmatrix} \frac{\partial \phi_x}{\partial \mathrm{x}} \\ \frac{\partial \phi_y}{\partial \mathrm{y}} \\ \frac{\partial \phi_x}{\partial \mathrm{y}} + \frac{\partial \phi_y}{\partial \mathrm{x}} \end{Bmatrix} \tag{2.49}$$

The resulting shear forces are thus [10]:

$$\begin{aligned} \begin{Bmatrix} Q_x \\ Q_y \end{Bmatrix} &= k \sum_{i=1}^{n} \int_{hi-1}^{hi} \begin{bmatrix} \bar{Q}_{44} & \bar{Q}_{45} \\ \bar{Q}_{45} & \bar{Q}_{55} \end{bmatrix} dz \begin{Bmatrix} {\gamma_{yz}}^0 \\ {\gamma_{xz}}^0 \end{Bmatrix} \\ &= k \begin{bmatrix} A_{44} & A_{45} \\ A_{45} & A_{55} \end{bmatrix} \begin{Bmatrix} \phi_y + \frac{\partial \mathrm{w}_0}{\partial \mathrm{y}} \\ \phi_x + \frac{\partial \mathrm{w}_0}{\partial \mathrm{x}} \end{Bmatrix} \end{aligned} \tag{2.50}$$

3 | EXPERIMENTAL PROGRAM

To gain even more knowledge regarding the specific buckling case of this study, practical experiments are performed. In the experimental test laboratory three tests were performed, one for each plate thickness (7.92, 5.31 and 2.49 mm).

In order to achieve compatible results, it is required to simulate the theoretical model as precise as possible and vice versa. Hence, it is of great advantage that scientists who study composite materials at *Centro de Engenharia e Tecnologia Naval e Oceânica (CENTEC)* benefit from the possibility of a experimental laboratory with several different test set-ups. The laboratory is capable of buckling experiments including the required clamped boundary conditions for this study.

3.1 Specimen Specification

Three different types of test specimens were ordered from the shipyard of *Estaleiros Navais de Peniche SA* in Portugal, in order to perform experimental plate buckling tests. Those three types of specimen plates have the same length and width but vary in their thickness. For each of those three thicknesses, all geometric specifications for the experimental tests are held constant throughout the computations for this work, in order to maximize comparability of results.
The specimens are produced with the vacuum bagging method to gain a high fibre volume fraction and thus optimize structural abilities while reducing weight.

3.1.1 Geometry

The specimens are produced in the three following thicknesses:

- 2.49 mm
- 5.31 mm
- 7.92 mm

The length and width of the three plates are identical for each specimen. The delivered plates have the following base dimensions, as also shown in figure 5.

- Real length: 320 mm (including clamped parts)
- Length: 200 mm (+60 mm clamped boundary condition on each side)
- Width: 50 mm

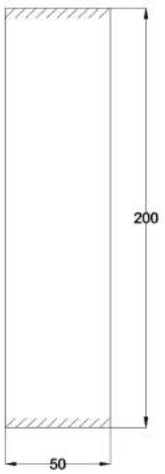

Figure 5: Test specimen geometry without clamped ends.

3.1.2 Specifications for Calculations & Tests

The specifications of the test specimens used for numerical and analytical computations are based on real values as they are based on mechanical property tests made with the specimen material.

- **Reinforcement Material:**
  - Fibre material: E-glass, 813 g/m2 per layer
  - Fibre constitution: Continuous, biaxial stitch
  - Producer/Company: Metyx Composites

- **Matrix Material:**
  - Resin Material: Crystic VE679PA vinylester resin
  - Producer/Company: Scott Bader

- **Lay-up Specification:**

Table 1 describes the lay-up sequence for each of the three plate thicknesses.

Table 1: Lay-up specification of test specimen

Thickness [mm]	No. of Layers [-]	Ply Thickness [mm]	Lay-up Sequence [°]
2.49	3	0.830	$[0]_3$
5.31	6	0.885	$[0]_6$
7.92	9	0.880	$[0]_9$

- **Material Properties:**
    - Young's Modulus: E_1 = 26400 MPa, E_2 = 25200, E_3 = 3000 MPa
    - Poisson Ratio: v_{12} = 0.24, v_{13} = 0.50, v_{23} = 0.06
    - Shear Modulus: G_{12} = 2200 MPa, G_{23} = G_{13} = 1200 MPa

3.2 Experimental Procedure

Prior to a practical experiment, a procedure shall be planned to avoid unnecessary errors and to make sure that all results are acquired following the same procedure. For this study, the following procedure was implemented throughout all three runs of the experiment.

The experimental procedure involves the following stages.

1. Preparation of specimen
    a. Preparing for strain gages (sanding, cleaning)
    b. Attaching strain gages to specimen (Gage type: 10 mm with two lead wires and 120 Ω resistance).
2. Installing of specimen in apparatus
    a. Attaching upper and lower clamps
    b. Correcting slight imperfections as far as possible
3. Installing dial gages
4. Attaching strain gages to computer
5. Start of hydraulic pump
6. Start of experiment (with connected software)
    a. Input speed of load cell
    b. Record video
    c. Take note of results
7. End of experiment
    a. Set load cell back to initial position
    b. Stop hydraulic pump
    c. Unscrew specimen and strain gages

3.3 Experimental Test Set-up

The apparatus of the composite material test laboratory is capable of applying the required boundary conditions of clamped ends to the test specimen. Further, it is possible to measure the in-plane displacements and the therefore resulting force applied to the plate. In order to measure the out-of-plane displacements we installed dial gauges on both sides of the installed test specimen to be prepared for the buckling case in any direction. The needles of the gauges were pointed perpendicular to the centre of the specimen surface to measure precisely lateral deflections.

To measure the longitudinal tensile and compressive strains, strain gauges were attached onto the centre of the specimen surface on both sides prior to the tests and connected to the computer to collect their measurements. A picture of the apparatus is shown in figure 6.

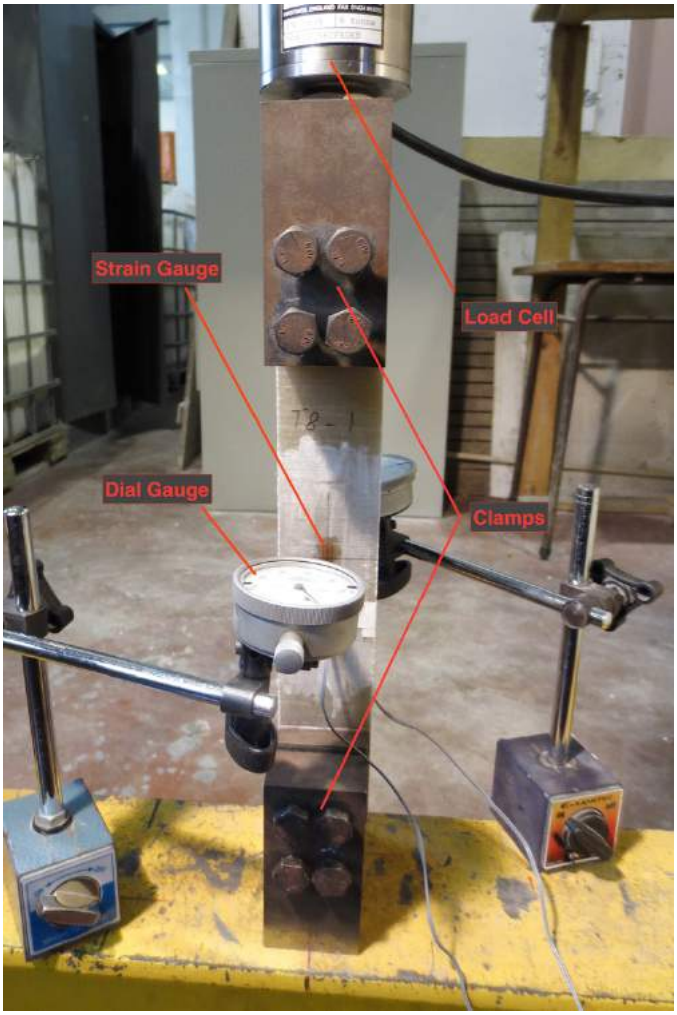

Figure 6: Apparatus and test set-up of the practical experiment.

4 | BUCKLING OF COMPOSITE PLATES

Buckling is a sudden failure case that can occur to a plate, a column or a bar that are subjected to normal loading. When this load exceeds a critical load value, sudden deflections and thus buckling occurs. In this chapter, this type of failure is specifically explained for the application in this study, which means buckling for composite plates under uniaxial compressive loading.

Buckling as a very important failure mode can be analysed in different ways in order to predict structural behaviour under compressive loading. To analyse structural components, researchers and engineers make most commonly use of tools like finite element analyses or analytical mathematical models. Another common possibility is to perform experimental tests. These tests are often combined with analytical or numerical calculations to validate theoretical results and possibly identify errors.

With the increasing use of laminated composite plates in various industries, the accurate knowledge of critical buckling loads, mode shapes and post-buckling behaviour is essential for the design process. The yacht building and marine industry often uses thin plate elements that are subjected to normal compression forces. Figure 7 shows the discretised model applied to this kind of problem for numerical and analytical computations.

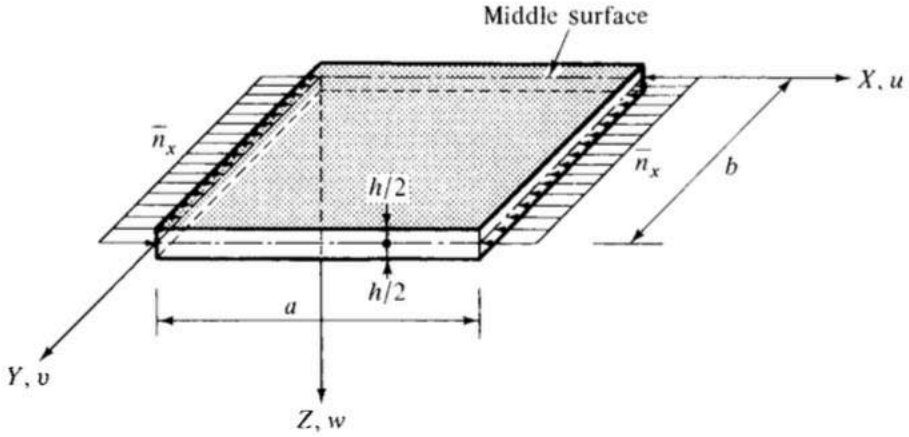

Figure 7: Rectangular plate subjected to in-plane edge loading. [4]

This input in form of in-plane forces or equivalent in-plane end-shortening causes deformations in different size and directions. If the input is small enough to result in in-plane displacements only, the state is described as stable (Case I in figure 8). As the magnitude of the input increases and reaches the critical buckling load, the state of equilibrium is so called neutral (Case II in figure 8).

Here, any increase of load input would lead to a sudden out-of-plane deflection. This state of equilibrium in case of an increase in input and the related deflection in z-direction is unstable (Case III in figure 8). [4]

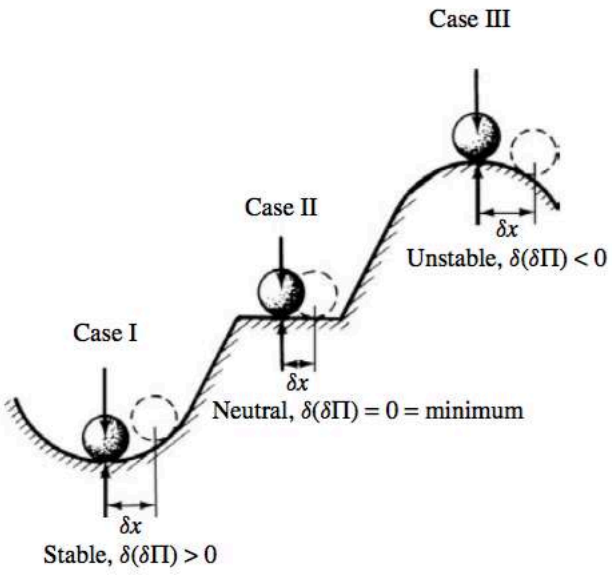

Figure 8: Buckling States of Equilibrium. [4]

Every buckling process that leads from a stable to an unstable equilibrium passes through a neutral state. This point is also called point of bifurcation (see figure 9) and is a very important point in structural design since engineers are trying to avoid exceeding this value. This critical buckling load splits buckling into pre- and post buckling. [4]

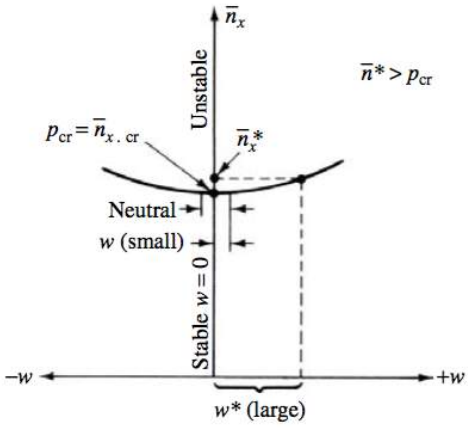

Figure 9: State of Bifurcation. [4]

However, the structure can still withstand greater loads before a total failure of the structural element occurs. The post-buckling analysis of flat plates is a difficult subject, since it is a non-linear problem that includes large deformations. [4]

Buckling can occur in different so called buckling modes (see in in figure 10). Each buckling mode is related to a different critical buckling load. In this study only the buckling mode for $n = 1$ is considered, since it relates to the smallest load or equivalent end-shortening. [4]

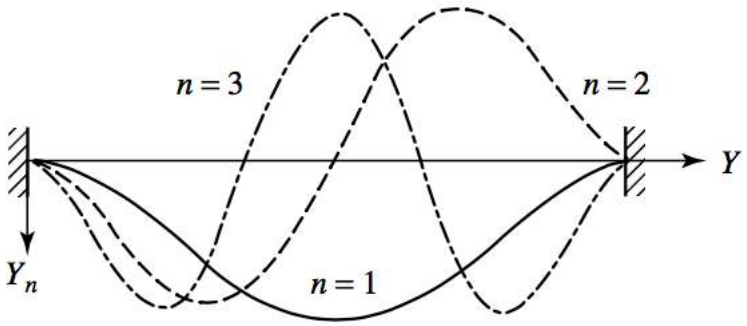

Figure 10: Buckling mode shapes of a clamped-clamped column. [4]

4.1 State of the art

While the main purpose of a buckling analysis generally is to predict the critical buckling load of structures, it is also very important to predict post-buckling behaviour. To do so, there are several different techniques and mathematical models to be chosen from. The two main categories are analytical and numerical calculations. Each of these two types offers many options within the method, in order to customize the analysis to special needs.
The most common way to perform a numerical analysis is to make use of finite element models. They have become one of the most accurate and thus widely used methods. Almost any geometry can be modelled and computed to the designer's preferences. However, the finite element method is not necessarily a problem free procedure. Shear locking of elements is the likeliest source of errors in finite element analysis that leads to higher buckling loads. [19]

In linear buckling analyses, the critical buckling loads are obtained by solving the eigenvalue problem of the stiffness matrix. Each eigenvalue is related to a critical buckling load of a specific buckling mode shape respectively. The smallest eigenvalue corresponds to the buckling initiation

value and usually to the mode shape of n=1 as shown in figure 5. An eigenvalue extraction algorithm suggested is Lanczos. It extracts multiple orders of eigenvalues in an efficient manner.
Linear buckling analyses neglect geometrical imperfection and thus usually overestimate the carrying capacity slightly. Since linear buckling models are highly efficient in computing terms, they are widely used to predict structural performance. [19]
Post-buckling analyses involve large deformations and need to apply a non-linear algorithm to predict structural behaviour. The main limitation of a non-linear analysis is the highly ineffective process of iteration during solving. [19]
For rather simple geometries, as the one present in this study, it is very common to make use of non-linear analysis because of the higher accuracy of results.
A more computing efficient alternative to numerical finite element models with acceptable accuracy are analytical methods. The majority of these methods are approximation models, which employ the energy principle to predict the critical buckling load or end-shortening value of structures. Commonly applied methods are the Rayleigh-Ritz, Galerkin or the Finite Strip method. Each of those methods implies orthotropic or anisotropic plate buckling theory for laminates, which are symmetrically stacked around the mid-plane axis. Unsymmetrically stacked laminates need more complicated models since they imply bending-stretching coupling. [19]
The Rayleigh-Ritz method is based on the energy variational principle. According to the theory, the potential energy should be minimal to make the equilibrium stable. Therefore, the derivatives of the potential energy with respect to the so called Ritz-Coefficients is set equal to zero and solved with a non-linear solving method. A crucial step in this method is the choice of displacement function because of their great influence on the final results. These functions can be of polynomial, trigonometric, hyperbolic or of spline type.

Several researchers study buckling and post-buckling behaviour of laminated composite plates. However, the specific combination of boundary conditions (CFCF) is rarely studied. A lot of information was found on finite element analysis of buckling of laminated composite plates with the software package of *Ansys*.

With respect to the chosen methods in this study, the most relevant milestones were set by the following list of studies.

In 1985, Leissa presented a report called “Buckling of Laminated Composite Plates and Shells”, which summarizes the technical literature on the subject to that date. It lists up several possible analytical approaches, governing differential equations, boundary conditions and types of shape functions. [14]

Seven years later, Dawe and Lam presented a “Non-linear Finite Strip Analysis of Rectangular Laminates under End-Shortening, using Classical Plate Theory”. For the finite strip analysis trigonometric shape functions are applied for the deflection shape assumptions. [15]

Turvey and Marshall published in 1995 the book called “Buckling and Post-buckling of Composite Plates”, which puts the work of leading researches together and describes in detail the established mathematical models and theories. Especially the Rayleigh-Ritz theory, plate theories are explained in detail with worked examples. [6]

The second edition of the book "Marine Composites" from Green in 1999 is a well rounded guide to overall knowledge of modern composite materials and its applications. The design processes are described in detail and structural abilities of various composite materials are listed up in great detail. [1]

In 2006, Bhagwan and colleagues published a book with the title “Analysis and Performance of Fibre Composites”. It provides the fundaments for mechanical calculations of composite structures and contains various worked examples for analytical and numerical calculations with detailed explanation. [2]

The following year, Reddy published the 2nd version of his book “Theory and Analysis of Elastic Plates and Shells”. It is a very complete guide to the subject of buckling of various geometric shapes and methods. [8]

In 2009, Yang released his master thesis “Simplified Approaches to Buckling of Composite Plates” in which he presents a simplified analytical approach for the plate theories of CLPT, FSDT and Higher-Order Shear Deformation Theory in combination with the potential energy minimization of Rayleigh-Ritz. The applied shape functions are of trigonometric type. The boundary conditions applied in the study are either completely clamped or simply supported. The mathematical model is limited to linear strains and the input is chosen to be of load type. A finite element analysis is done with the software of *Ansys* and a comparison with the analytical results is presented. [10]

In the same year, Kharazi and Ovesy published a paper on buckling of laminated composite plate buckling and delamination. Theories of CLPT, FSDT and HSDT are applied to a mathematical model in combination with polynomial shape functions. The Rayleigh-Ritz minimizing potential energy method is applied to solve the buckling problem. The mathematical model makes use of end-shortening as input. [9, 20, 21]

Barbero released in 2010 the 2nd edition of his book “Introduction to Composite Materials Design”. It contains mechanical design of composite structures, fundamental knowledge of composite materials and explanations of modern procedures to produce composite materials. [16]

In 2010, Ovesy and Kharazi published a conference paper called “Buckling of Composite Laminates with Through-The-Width Delamination Using a Novel Layerwise Theory”. The work

applies FSDT and polynomial shape functions in combination with the Rayleigh-Ritz method to a mathematical model. Further, it makes use of Green-Lagrange non-linear strains and end-shortening as input. [11]
Further, Xu and Zhao released in 2013 a paper about “A Critical Review on Buckling and Post-Buckling Analysis of Composite Structures”. The article lists up the most common approaches to buckling analyses with its advantages and disadvantages. [7]
In 2014, Pankajkumar released his master thesis with the title “Free Vibration and Buckling Behaviour of Laminated Composite Panels under Thermal and Mechanical Loading". The work consists analytical calculations including CLPT and FSDT as well as numerical computations done in *Ansys.* [5]

No research was found on the analytical approach of applying trigonometric shape functions with the Rayleigh-Ritz method in combination with the present boundary conditions and end-shortening as input. Therefore, it is safe to say that the present study fills a gap in research.

4.2 Buckling Analysis

4.2.1 Analytical Approach

Based on the theoretical foundations of chapter 2 mathematical computation code in the software of *Maple* is written. The code is divided in two different programs, one applying the theory of CLPT and the other FSDT. Each of the programs are performing computations based on the same boundary conditions and same energy variation principle. The purpose of the development of two programs, which only vary in the applied plate theory, is to compare the influence of the theories on the final results.
The mathematical code uses uniaxial compressive end-shortening as input. It is further capable of computing not only buckling initiation but also post-buckling behaviour. To calculate the minimum buckling load, the minimizing potential energy method of Rayleigh-Ritz is chosen. The problematic of non-linearity is eventually solved by applying the Newton-Raphson method. The following graphic in figure 11 shows a 2D schematic of the mathematical model including the applied end-shortening.

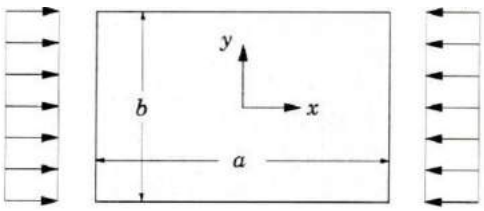

Figure 11: Clamped-clamped plate under uni-axial compressive load. [10]

Boundary conditions for both plate theories are equal and of clamped-clamped type. The unloaded opposing two edges of the rectangular plate are free. This particular set of boundary conditions can be described as “clamped-free-clamped-free”. With two “free” edges, the problem can be simplified to a 2D model of deflections while it has to contain the mechanical properties of a 3D plate. Typically, the buckled shape of the first buckling mode is as in figure 12.

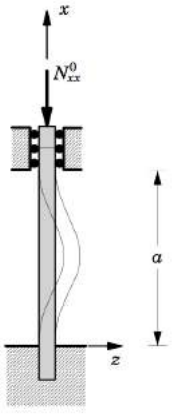

Figure 12: First buckling mode shape of a clamped-clamped column. [10]

The boundary conditions of the four plate edges are split up in two different types for each edge, geometrical (5.1, 5.2) and statical (5.3 – 5.6) boundary conditions:

- Geometrical Boundary Conditions (Edge displacement in z-direction) [4]:

$$w(x = 0) = \frac{\partial \mathrm{w}}{\partial \mathrm{x}} = 0 \tag{4.1}$$

$$w(x = a) = \frac{\partial \mathrm{w}}{\partial \mathrm{x}} = 0 \tag{4.2}$$

- Statical Boundary Conditions (Edge moment and edge shearing force in y-direction) [4]:

$$M_y(y = 0) = \left(\frac{\partial^2 w}{\partial x^2} + v\frac{\partial^2 w}{\partial y^2}\right) = 0 \tag{4.3}$$

$$M_y(y = b) = \left(\frac{\partial^2 w}{\partial x^2} + v\frac{\partial^2 w}{\partial y^2}\right) = 0 \tag{4.4}$$

$$v_y(y=0) = \left[\frac{\partial^2 w}{\partial x^2} + (v-2)\frac{\partial^3 w}{\partial \mathrm{x}\,\partial y^2}\right] = 0 \tag{4.5}$$

$$v_y(y=b) = \left[\frac{\partial^2 w}{\partial x^2} + (v-2)\frac{\partial^3 w}{\partial \mathrm{x}\,\partial y^2}\right] = 0 \tag{4.6}$$

4.2.1.1 Calculations with CLPT Method

For both plate theories the energy method of Rayleigh-Ritz is chosen in order to solve the buckling problem. This method requires an initial assumption for the deflection shapes. The two most common approaches for this solution are polynomial and trigonometric terms. As advised by [4], the shape functions of the assumed solution are chosen of trigonometric type. Further, we neglect the term that describes the shape function in y-direction, since we assume the critical buckling load will occur without deformations in y-direction.

A trigonometric out-of-plane deflection shape function in z-direction that satisfies the given boundary conditions is [4]:

$$w = \sum_{i=1}^{M} c_i \left(cos\left(\frac{2i\pi x}{a}\right) - 1\right) \tag{4.7}$$

The expression of the in-plane displacement in x-direction is assumed to be the following [15]:

$$u = -\frac{ep}{a} * x + \sum_{i=1}^{M} d_i \, sin\left(\frac{i\pi x}{a}\right) \tag{4.8}$$

where ep is the applied end-shortening.

where the so called Ritz-Coefficients c_i and d_i need to be determined to receive the final shape function including its amplitude. The choice of the shape function is of major importance for the quality of the final result of the buckling problem.
Results are also highly dependent on the amount of degrees of freedom. If a high number of degrees of freedom is chosen, the results will be of high accuracy but computation time will be less efficient. Are they chosen too low, then the results are most likely too low. It is important to find a compromise related to this variable that leads to sufficient accuracy. In this study the amount of degrees of freedom is chosen to be seven $M = 7)$.

In order to apply the Rayleigh-Ritz Method, it is required to formulate the energy functional. The strain energy of laminated plates is given matrix form in the following equation [6].

$$\Pi = \frac{1}{2}\iint \begin{Bmatrix}\{\varepsilon\}\\ \{\psi\}\end{Bmatrix}^T \begin{bmatrix}[A] & [B]\\ [B] & [D]\end{bmatrix} \begin{Bmatrix}\{\varepsilon\}\\ \{\psi\}\end{Bmatrix} = 0 \tag{4.9}$$

where $A_{ij,}\, B_{ij}$ and D_{ij} are the stiffnesses over the thickness of the laminated composite plates. [6]

The composite plates of this study are of especially orthotropic laminate type. For this type, the equations allow us to be simplified as follows [10]:

$$A_{16} = A_{26} = 0 \tag{4.10}$$

$$B_{ij} = 0 \tag{4.11}$$

$$D_{16} = D_{26} = 0 \tag{4.12}$$

Taking these assumptions into account, the energy equation eventually becomes:

$$\Pi = \frac{1}{2}\int_0^a \int_0^b A_{11}\varepsilon_l^2 + A_{11}\varepsilon_{nl}^2 + 2\,A_{11}\varepsilon_l\varepsilon_{nl} + D_{11}\psi^2\, dy\, dx \tag{4.13}$$

The method of Rayleigh-Ritz requires for the equilibrium that the potential energy term derived to each of the Ritz-Coefficients is equal to zero [6].

$$\frac{\partial \Pi}{w_i} = \delta w_i = 0 \tag{4.14}$$

Thus [6],

$$\frac{\partial \Pi}{w_i} = 0 \tag{4.15}$$

After deriving the potential energy functional with respect to every degree of freedom, a set of equilibrium equations result. These equations are of non-linear type and need to be solved with an appropriate method. For this study, the Newton-Raphson iterative method is chosen to solve the equations. To receive converging results for all degrees of freedom, it is necessary to make initial estimated of sufficient quality.

Once the non-linear global equilibrium equations are solved for a chosen value of end-shortening, the shape initially introduced estimate functions of w and u can be calculated and plotted.
The CD handed with this dissertation includes the full *Maple* computation code of the CLPT, which includes every detail of the computations.

4.2.1.2 Calculations with FSDT Method

The boundary conditions of the four plate edges are the same as for CLPT. For best comparability, it is also chosen Rayleigh-Ritz energy minimization method to solve the problem.

The out-of-plane buckling shape function in z-direction of trigonometric type is chosen to be the following [4].

$$\mathrm{w} = \sum_{i=1}^{M} c_i \left(cos\left(\frac{2i\pi x}{a}\right) - 1 \right) \tag{4.16}$$

The expression of the in-plane displacement in x-direction is assumed to be the following [15].

$$\mathrm{u} = -\frac{ep}{a} * x + \sum_{i=1}^{M} d_i \, sin\left(\frac{i\pi x}{a}\right) \tag{4.17}$$

The expression of the rotation about the x-axis is assumed to be the following [15].

$$\phi_x = \sum_{i=1}^{M} e[i] \, sin\left(\frac{i\pi x}{a}\right) \tag{4.18}$$

As previously for CLPT, the Ritz-Coefficients $(c, d \text{ and } e)$ need to be determined for every degree of freedom to receive the final shape function depending on the amount of degrees of freedom.

The energy functional needs to be formulated to apply the Rayleigh-Ritz. The strain energy of laminated plates is given in matrix form in the following equation [6].

$$\Pi = \frac{1}{2} \iint \begin{Bmatrix} \{\varepsilon\} \\ \{\psi\} \\ \{\gamma\} \end{Bmatrix}^T \begin{bmatrix} [A] & [B] & 0 \\ [B] & [D] & 0 \\ 0 & 0 & [A_s] \end{bmatrix} \begin{Bmatrix} \{\varepsilon\} \\ \{\psi\} \\ \{\gamma\} \end{Bmatrix} = 0 \tag{4.19}$$

where $A_{ij,}\, B_{ij}$ and D_{ij} are the stiffnesses over the thickness of the laminated composite plates.[6]

As previously for the CLPT method, the composite plates of this study are of especially orthotropic laminate type. For this type the equations allow us to be simplified as follows [10]:

$$A_{16} = A_{26} = 0 \tag{4.20}$$

$$B_{ij} = 0 \tag{4.21}$$

$$D_{16} = D_{26} = 0 \tag{4.22}$$

Eventually, the energy expression for the method of FSDT becomes:

$$\Pi = \frac{1}{2}\int_0^a \int_0^b \varepsilon_0^T A\varepsilon_0 + \varepsilon_1^T A\varepsilon_1 + \varepsilon_0^T B\varepsilon_1 + \gamma^T A_s \gamma \, dy \, dx \tag{4.23}$$

The method of Rayleigh-Ritz requires for the equilibrium that the potential energy term derived to each of the Ritz-Coefficients is equal to zero [6].

$$\frac{\partial \Pi}{w_i} = \delta w_i = 0 \tag{4.24}$$

Thus [6],

$$\frac{\partial \Pi}{w_i} = 0 \tag{4.25}$$

As for the CLPT method, this results in a set of non-linear equations that are required to be solved for the final result.

After applying the Newton-Raphson iterative method, the non-linear global equilibrium equations are solved for a chosen value of end-shortening. In the next step, the shape initially introduced estimate functions of ϕ_x, w and u can be calculated and plotted.

The CD handed with this dissertation includes the full *Maple* computation code for the FSDT, which includes every detail of the computations.

5 | FINITE ELEMENT INVESTIGATIONS

5.1 Principles of Finite element method

The finite element analyses (FEA) performed in this thesis are based on the software of *Ansys, version 11.* This software enables the user to make use the finite element computational technique via a user interface. This chapter briefly outlines the theoretical foundations of the main computation procedures.

Finite element methods are computation techniques that approximate solutions. Therefore, in the software any physical structure is represented in form of elements. Depending of the aim of analysis and of the physical characteristics different element types and geometric representations can be chosen from.
A finite element computation usually requires at least three types of input, geometry, material values and a form of loading. The finite element program transforms the input of this information to an element stiffness matrix. The size of the stiffness matrix depends on the chosen mesh size and element type. The material constants reflect the resistance of the element to deformation that results from the loading.

The three main steps during a FEA are [13]:

1. ***Pre-processing:*** The user develops geometry of the model that is aimed to be analysed. Then this model is refined in sub regions, depending on the element type and mesh refinement.
2. ***Analysis:*** The finite element software uses the dataset of the *pre-processor* as input to the finite element code itself. Depending on the analysis type a system of linear or non-linear equations is constructed and solved.

$$[K_{ij}]\{u_j\} = \{f_i\} \tag{3.1}$$

Where $[K_{ij}]$ is the element stiffness matrix, $\{F_i\}$ is the vector of applied forces and $\{u_j\}$ the displacements. The stage of *Analysis* is a very crucial step during a buckling analysis and should be split up in three steps.

- ***Static Linear:*** This type of analysis assumes the structure and thus the finite element model to behave linearly. Further, only small deflections are considered.

- ***Static Eigenvalue Buckling:*** This analysis represents the buckling analysis according to Euler. It predicts the critical buckling strength of the finite element structure. During this type of Analysis different eigenvalues are computed. Each of those eigenvalues represents the critical buckling load for a related buckling mode.
- ***Static Non-Linear:*** This analysis type takes non-linearity into account. This non-linearity can represent material, geometric or contact properties. Large deformations are considered. This analysis type is the especially important for a post-buckling analysis and thus fundamental for this study. The resulting system of non-linear equations is solved by implementing the Newton-Raphson method.

3. **Post-processing:** In this stage the results of the *Analysis* are transformed into useful data. The broad set of acquired numbers is transformed to nodal displacements, reaction forces, stresses, strains, etc.

5.2 Finite Element Buckling-Analysis

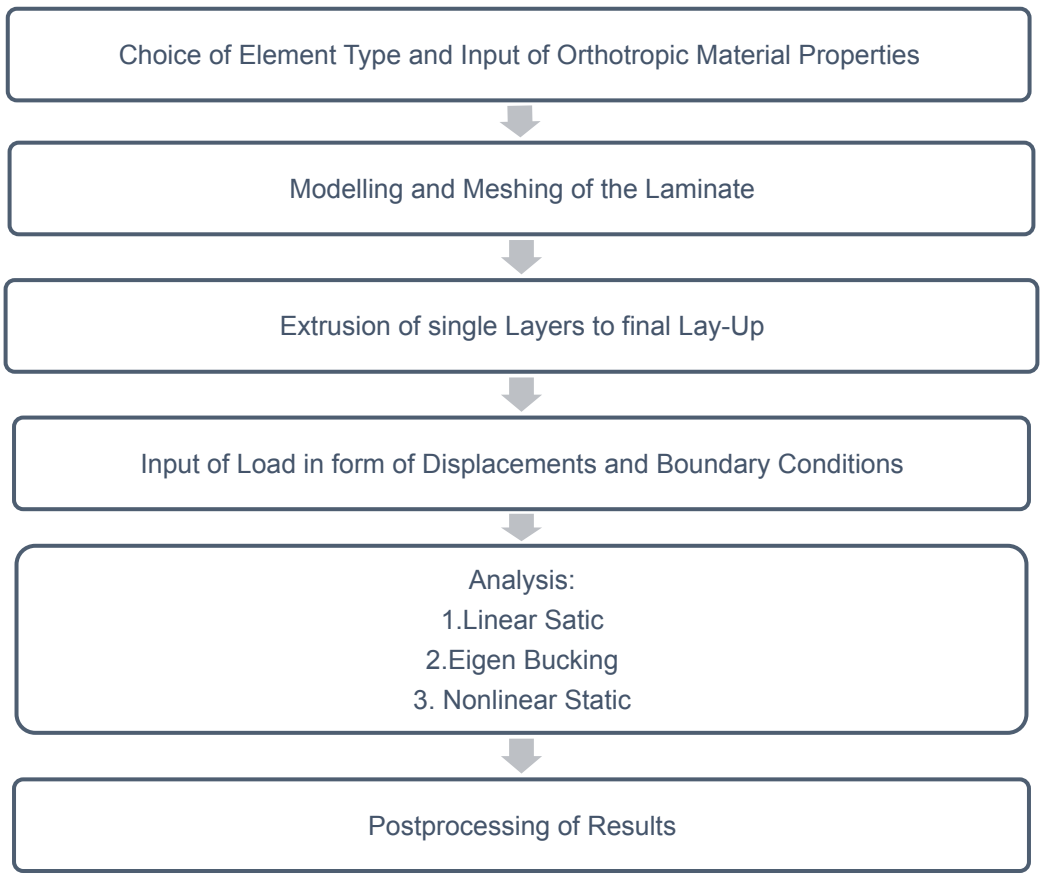

Figure 13: Flow chart load of model in the software of *Ansys*.

A series of finite element computations are realized with the same input data of the composite plates previously described in the specimen specifications. The software chosen for this simulation is the software package of *Ansys* version 11. *Ansys* is a powerful finite element computation tool with a great range of element types. With the purpose of verifying and comparing the previous analytical methods, a finite element model is developed as described in this chapter. The main procedure in the program of *Ansys* is described by the following flow chart.

5.2.1 Finite Element Model

The development of a finite element model involves many steps, in which choices are needed, that can influence the final results drastically. Therefore, this chapter lists up the most important necessary steps and settings in the computation procedure. The CD handed with this dissertation includes the detailed description in form of a command history of the procedure and the involved choices. The following procedure is modelled and computed in *Ansys APDL*.

1. The first crucial step during the finite element modelling is the choice of an element type. Chapter 6 handles a detailed study on the different relevant Solid 3D structural element types of the software. For this chapter, the computing efficient and accurate element type of *Solid 46,* which is a layered version of *Solid 45,* is chosen.

2. Material properties are brought into the model as “linear – elastic – orthotropic”. The material properties can be found in the specimen specification of chapter 4.2.

3. In the next step, it is necessary to develop the plate geometry. This can be achieved in various different ways with the exact same result. Here, it was chosen to model the 2D geometry of the composite plates plane area at first and extrude it afterwards to achieve a 3D model. Each ply of the composite plate is modelled separately. In a later step of the model the single plies are merged together by merging their nodes. In this model the geometry is modelled including the clamped parts of the real tests specimen resulting in an additional length of 60 mm on each loaded edge. The centre of the coordinate system is chosen to be in the centre of the plates surface.

4. Meshing of the model is another crucial point during the development of a finite element model. The mesh should be chosen not too fine, not too coarse in order to achieve high accuracy and acceptable computation time. Chapter 6 handles a detailed study regarding the mesh size. In rather complex geometries, it makes sense to define parts with finer or coarser mesh areas to optimize computation times and results. In this study

however, the geometry is constant and no mesh simplifications can be allowed. The mesh size was chosen to of 1 mm space in between each node in x- and y-directions. In z-direction the mesh is chosen to be depending on the ply thickness and thus be one element per composite ply.

5. Boundary conditions are of major importance to simulate the same conditions as in analytical and in experimental approach. In *Ansys* this is commonly done by constraining displacements and rotations. This can be achieved by applying "structural displacements" on chosen nodes. In this particular model the geometry and the constraints in displacement are applied to the nodes of the additional length of the clamped parts of the plates. This aims to simulate the boundary condition of the clamped-clamped test apparatus of the experimental tests. In this stage of modelling, the end-shortening is assigned to the model. A total value of 2 mm in end-shortening is split up equally on the opposing loaded edges.

   The applied structural displacements to the model are the described as follows and are shown graphically in figure 14. The two opposing loaded edges are clamped while a displacement in x direction is applied on each side of 1 mm (2 mm total displacement).
   In the FEA software of *Ansys* this is simulated by applying structural displacement as follows.

   i. At nodes from $+100\,mm$ to $+160\,mm$ the displacements applied are: $UZ = 0\,mm$, $UX = -1\,mm$ on all nodes and $UY = 0\,mm$ on the centre nodes ($y = 0\,mm$) only.
   ii. At nodes from $-100\,mm$ to $-160\,mm$ the displacements applied are: $UZ = 0\,mm$, $UX = +1\,mm$ on all nodes and $UY = 0$ mm on the centre nodes ($y = 0\,mm$) only.

Figure 14: Applied boundary conditions in form of structural displacements in mm for a clamped-free-clamped-free plate in *Ansys*.

At this stage the modelling part is finished and a range of analyses are possible. For this study, it is chosen a combination of three types of analyses that need to be executed in the following order.

6. In the first step of the analyses, a static analysis is executed.

7. Once the solution is completed, the static analysis is followed by an eigenvalues buckling analysis. Here the “Block Lanczos” method is chosen in combination of five buckling modes.

8. The buckling eigenvalue analysis is followed by a large-deflection, non-linear analysis. A total of 20 sub-steps are chosen. For the solving process of the convergence analysis a maximum of 150 iterations per sub-step is determined. Following this procedure, the outcome is the final results of the finite element analysis.

5.3 Calculations in Ansys: Element Analysis

During a finite element analysis in *Ansys 11,* one gets confronted with the choice of element type. Different element types usually result in varying results. Consequently, it is of utmost importance to understand the differences of element types and their most suitable applications.
For the present problem the list of available elements is already narrowed down by the physical field of Structural Analysis.
Solid elements in *Ansys* are elements with displacements of degrees of freedom only, which means that no rotational degrees of freedom are possible. The Solid element types in the Program of *Ansys 11* are split up into three main groups. [17]

- Shell 2D
- Plane 2D
- Solid 3D

In this study, only the third group of Solid 3D elements are investigated. The relevant Solid 3D element types in the software of *Ansys 11* to be investigated are the following. [17]

- Solid 45
- Solid 46
- Solid 185

- Solid 186
- Solid 95
- Solid 64

5.3.1 Approach

An investigation of this kind has to be performed under the same conditions each time. Consequently, a procedure is chosen according to the finite element analysis explained in chapter 5.3

Boundary conditions and mesh sizes are held constant throughout this experiment and is chosen to be as described earlier on in Chapter 5.3. In addition, one of the three previously investigated plate thicknesses is chosen for this subject

As an initial mesh size the corner lengths of 1x1 millimetres squares are chosen in the directions of x and y. This results in an overall amount of 320 and 50 elements in the directions of x and y respectively. The 5.31 mm thick plate enclosing 6 layers of composite fibres is assumed to be most suitable for this comparison. Accordingly, to the lay-up a total amount of 6 elements in z-direction is chosen with an edge length of 0.885 mm of each element.

5.3.2 Element Type Definitions

A brief description of the investigated element types is introduced in this chapter. For any more detailed information about each plate element [17] can be consulted.

The chosen element types can be divided into two groups, the lower order and the higher order elements. For most elements the program of *Ansys* contains a lower and a higher order version and for some it contains a third, the layered version. For instance, the Solid 45 element is the lower order version of the element Solid 95 and the layered version of Solid 45 is Solid 46. [17]

The main difference is that the higher order elements have 20 nodes, while the traditional, lower ones contain only 8 nodes. This means that in between each two nodes of the lower order elements an additional node exists in the higher order versions. One reason for that is that the lower order elements tend to encounter errors like locking that can be corrected by applying the higher order types.

The two most common locking error types are shear locking and volumetric locking.

Shear locking might occur with the lower order element types since the geometry only allows for linear lines as edges. Therefore, parasitic shear strains occur. Thus, the traditional elements are too stiff for the case of pure bending for instance. [18]

Volumetric locking is a function of the material and only occurs with nearly incompressible materials. This is not the case for composite materials and is thus not relevant for this study. [18]

The element type of Solid 45 (3D 8-Node Structural Solid) is used to model Solid structures in 3D. It is a lower order element and thus defined by 8 nodes of which each has three degrees of freedom in the directions of x, y and z. The element is capable of handling plasticity, swelling, creep, stress stiffening, large deflection and large strain. Further, it handles orthotropic materials in relation to the three main degrees of freedom. [17]

The Solid 46 (3D 8-Node Layered Structural Solid) element type is an extended the structural 8-Node Solid 45. Solid 46 is especially designed to model layered thick shells or Solids of up to 250 layers. The element is defined by 8 nodes of which each node has three degrees of freedom in the directions of x, y and z. As well as Solid 45, Solid 46 is capable of computing plasticity, swelling, creep, stress stiffening, large deflection and large strain. It handles orthotropic materials in respect to the three main degrees of freedom, as well.. [17]

The Solid 64 (3D 8-Node Anisotropic Solid) element type is developed to model anisotropic Solid structures of three-dimensional type. It is a lower order element defined by eight nodes with three degrees of freedom for each in form of translation. Further, it is defined by the anisotropic or orthotropic material properties. The element has capabilities for handling stress stiffening and large deflections. This type of element is convenient for various applications such as crystals or composites. Due to many similarities Solid 95 shall be chosen if a higher order element type would be necessary.[17]

Solid 95 (3D 20-Node Structural Solid) is a higher order element type based on the lower order version element type Solid 45. It tolerates irregular shapes without a major loss of accuracy. It is defined by 20 nodes per element with three degrees of freedom for each in the directions of x, y and z. The elements capabilities are plasticity, creep, stress stiffening, large deflections and large strains.[17]
Solid 95 is an element type that tolerates irregular shapes without major losses in accuracy. The reason for this is that it is a higher order element type that has compatible displacement shapes. It is thus well suited to model curved boundaries. [17]

This element type Solid 185 (3D 8-Node Structural Solid or Layered Solid) is another suitable lower order, 3D structural element defined by eight nodes with three translation directions for each node in the directions of x, y, and z. The element allows plasticity, hyper elasticity, stress stiffening, creep, large deflection and large strain. Further, it has mixed formulation capabilities to allow simulating deformations of nearly incompressible elastoplastic materials and fully

compressible hyperelastic materials. Alternative element types are Solid 45 and Solid 64 as advised by [17]. Solid 95 is suitable as a higher order element if needed. [17]

Solid 186 (3D 20-Node Structural Solid or Layered Solid) is an element type of higher order including 20-nodes with three degrees of freedom of translation type in the directions of x, y and z. The element exhibits quadratic displacement behaviour. It supports plasticity, hyper elasticity, creep, stress stiffening, large deflection and large strain. [17]

5.4 Calculations in Ansys: Mesh Size Comparison

An additional study is performed to gain knowledge of the effect of different mesh sizes on the numerical computation results. For this study, the element type Solid 45 is chosen to be investigated. Solid 45 delivers a very high accuracy combined with the fastest computation time.

The mesh corner lengths are defined as a, b and c, representing the corner lengths in x, y and z respectively. The mesh size in the direction of y and thus corner lengths of b are held at a constant value of one mm throughout this investigation. The focus of this study lies on the element size in the directions of x and z.
As an indicator of result precision, the out-of-plane deflection in z-direction is chosen. To receive unmistakeable, results are noted for the surface node in the centre of the plate.
Since mesh effects are studied in two different axes, the investigation is split up into two parts, the effect of mesh size in x- and z-direction. Precisely, mesh lengths in x-direction are investigated in the range of 0.5 to 10 mm, in z-direction from 0.885 to 5.31.
As an example, the following figure 15 represents the finest calculated mesh geometry of this study.

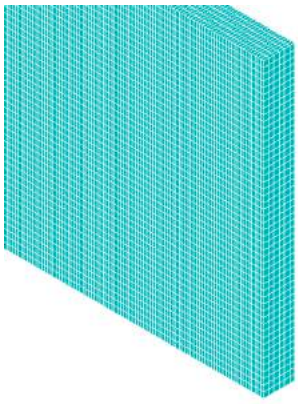

Figure 15: Finest calculated mesh geometry of this study.

6 | ANALYSIS OF RESULTS

This chapter lists up results of the applied methods and studies of the previous chapters. Results are reported for the analytical, numerical, experimental buckling analysis and for the element and mesh size investigation.

6.1 Analytical, Numerical and Experimental Buckling Analysis

The results of the analytical methods of CLPT and FSDT are compared to the numerical approach of *Ansys* and experimental. This is done in order to compare the results and thus the applied methods with each other for each plate thickness. For all approaches the compressive and tensile strain results are plotted for each of the three plate thicknesses and compared with each other. In addition to that, the out-of-plane displacement shapes of CLPT, FSDT and *Ansys* are plotted together for a fixed end-shortening value of u = 1.5 mm for each plate thickness.
More details of the results and the related tables can be found in the spread sheet handed with this thesis.

6.1.1 Out-of-plane vs. in-plane displacements

The following plots (figure 16, 17 and 18) are presenting the resulting out-of-plane displacement from the input of end-shortening type.

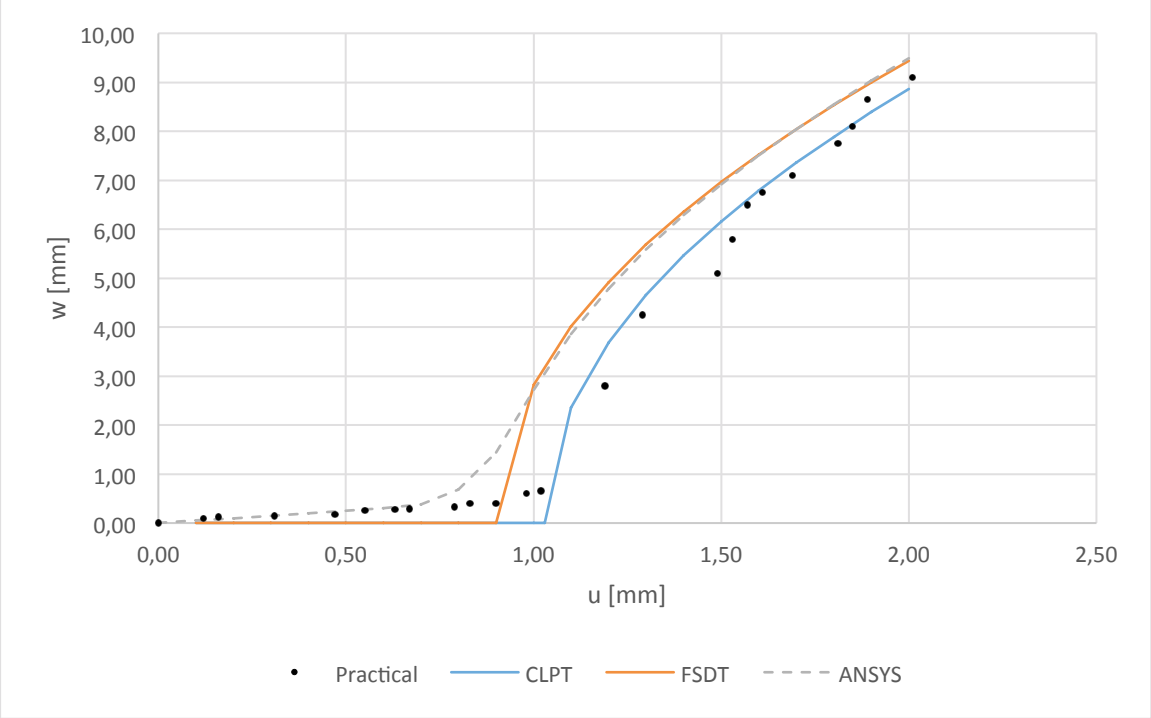

Figure 16: Displacement results for t = 7.92 mm

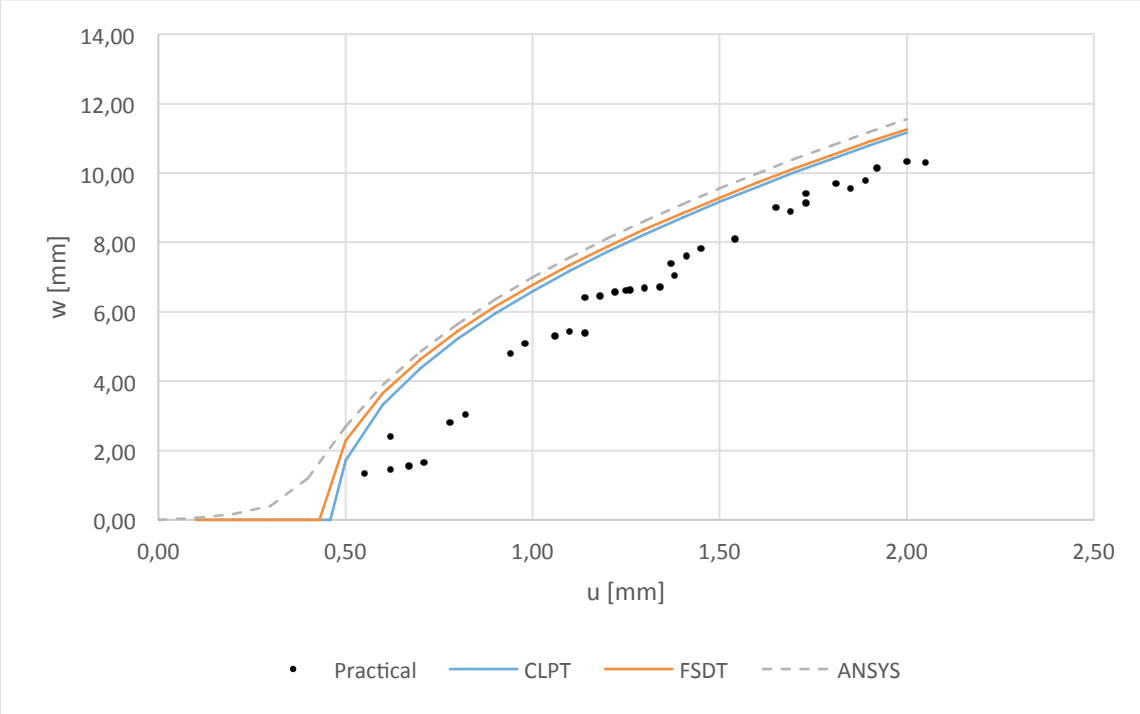

Figure 17: Displacement results for t = 5.31 mm

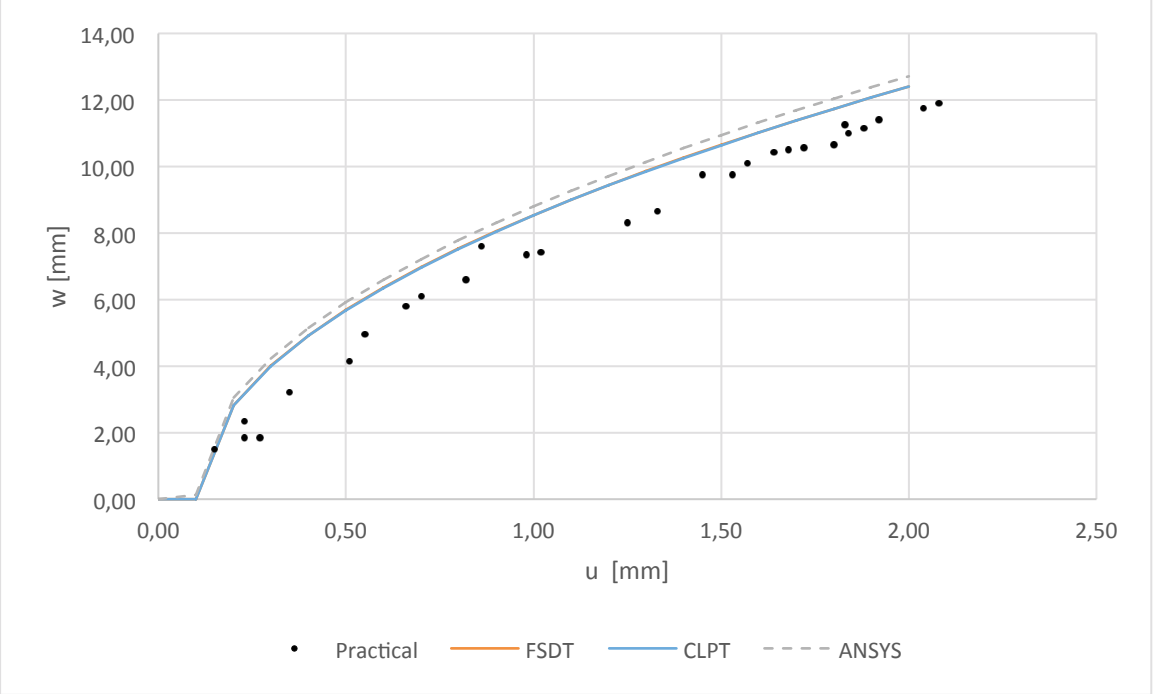

Figure 18: Displacement results for t = 2.49 mm

Furthermore, table 2 presents the results of the corresponding discrepancies in form of relative errors over the different plate thicknesses and computation methods.

Table 2: Relative Errors for u = 1.5 mm

Plate Thickness [mm]	CLPT - FSDT	CLPT - ANSYS	FSDT - ANSYS
7.92	13,07	12,35	0,64
5.31	1,36	4,20	2,81
2.49	0,05	2,80	2,75

6.1.2 Strains resulting from in-plane displacement

For each plate thickness the results for the strains on the compressive and tensile surface of the plates are plotted together for the analytical, numerical and experimental approaches (see figure 19, 20 and 21), divided into the different plate thicknesses.

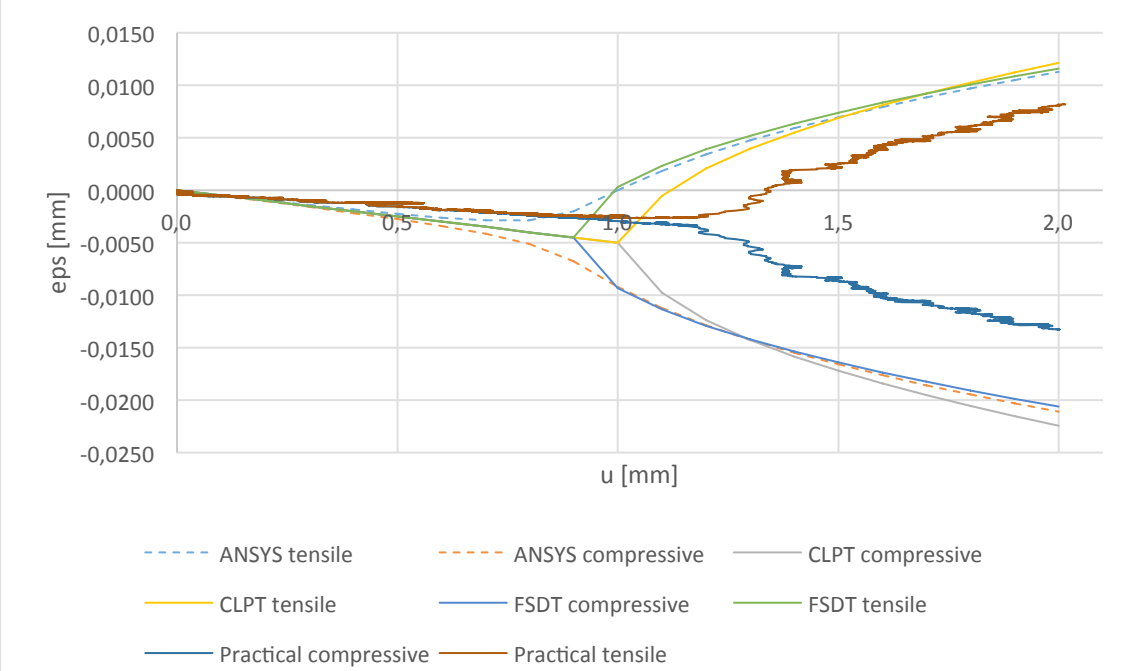

Figure 19: Compressive and tensile strain results for t = 7.92 mm

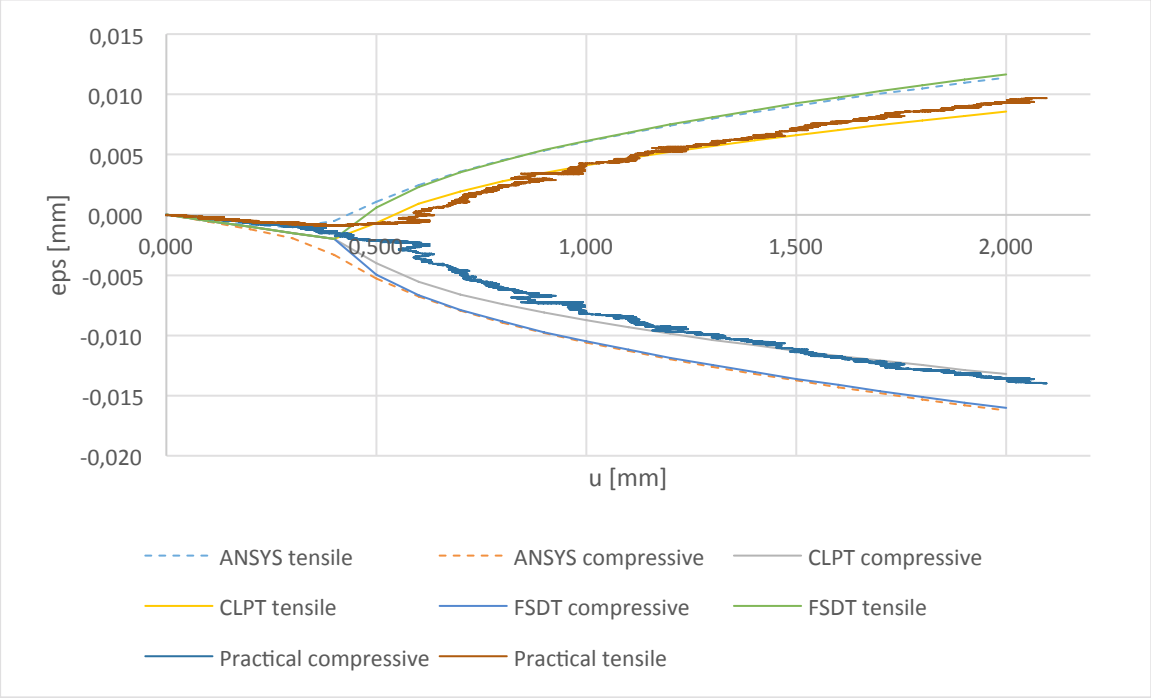

Figure 20: Compressive and tensile strain results for t = 5.31 mm

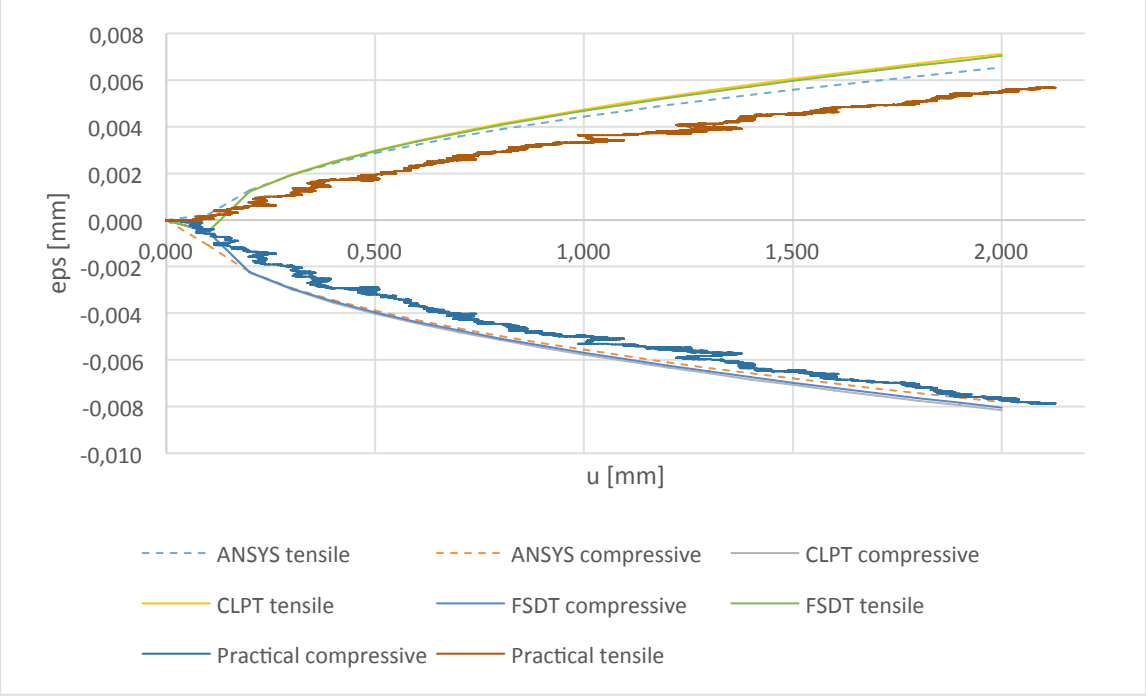

Figure 21: Compressive and tensile strain results for t = 2.49 mm

6.2 Finite Element Analysis

The results of the study of different structural 3D element types are listed up and compared with each other. The entire element comparison is based on the plate thickness of 5.31 mm. Elements are compared with each other for three different mesh sizes in x-direction (1 mm, 2 mm and 5 mm).

Results are gained and compared for out-of-plane resulting from in-plane displacement (figure 22, 23 and 24). Strains for compressive and tensile side of the plate are shown in appendix in figure 34, 35 and 36. In addition to that, the out-of-plane displacement shape is calculated and presented in the appendix in the tables 7, 8 and 9.

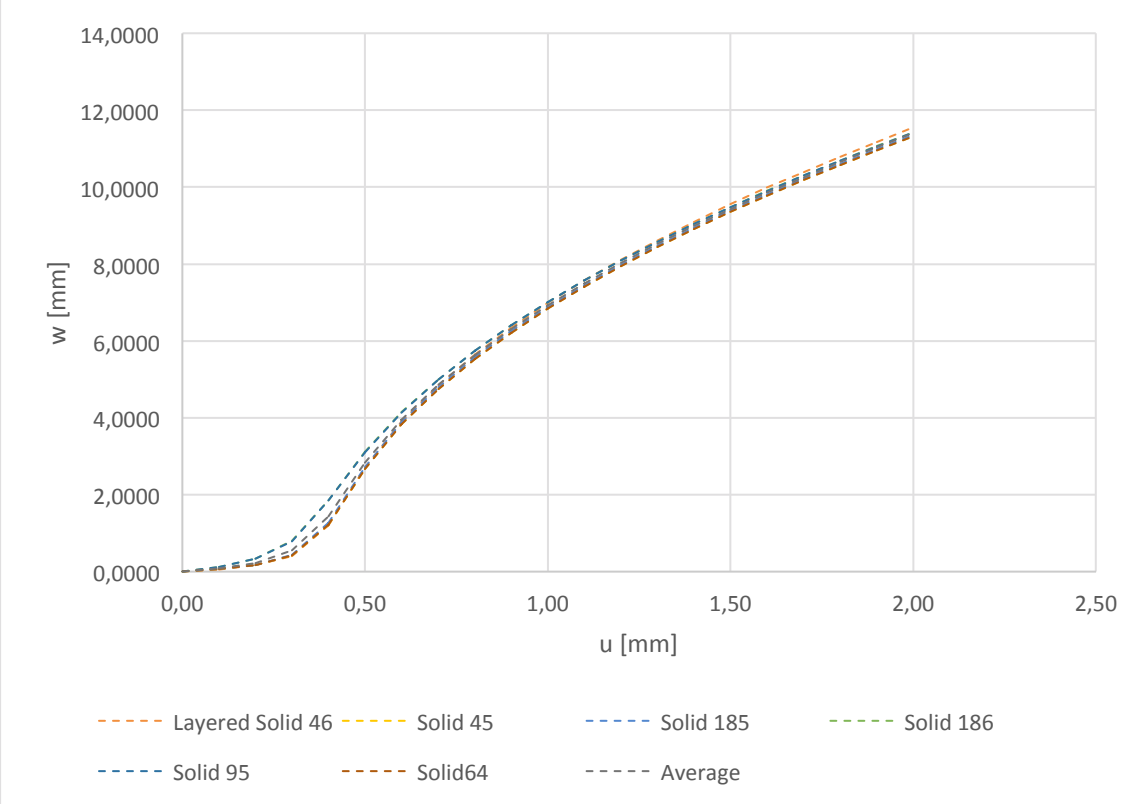

Figure 22: w-deflections for element length of 1 mm in x-direction (t = 5.31 mm).

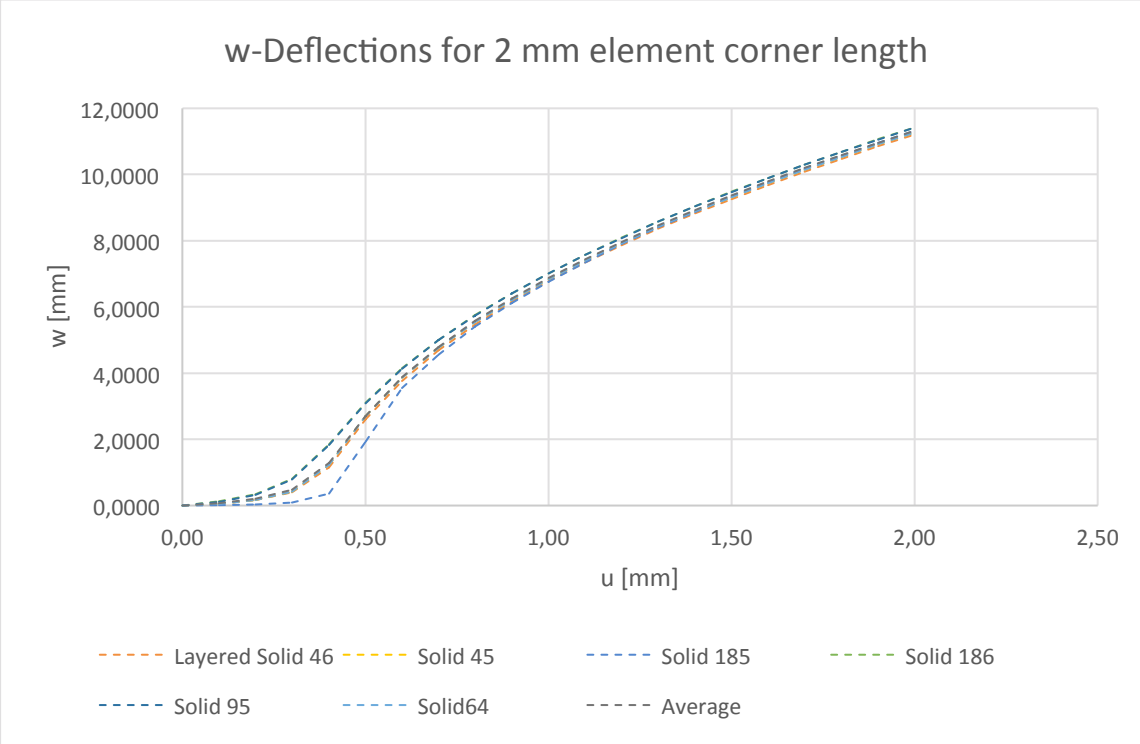

Figure 23: w-deflections for element length of 2 mm in x-direction (t = 5.31 mm).

Figure 24: w-deflections for element length of 5 mm in x-direction (t = 5.31 mm).

6.3 Mesh Size Analysis

For each element type the mesh size is varied in x-direction in order to gain knowledge about the influence of the element corner length in x-direction. Afterwards, to acquire even more detailed information about the mesh size effects, the element of Solid 45 is chosen to be compared in even more mesh size variations in x-direction and in a additional detailed investigation of the mesh size in z-direction.

6.3.1 Mesh size Influence in x-direction for different element types

Here, the results for each considered element types are compared with respect to the mesh size in x-direction. The three investigated mesh sizes are 1 mm, 2 mm and 5 mm in x-direction.

The out of plane deflections for varying mesh sizes in x-direction are plotted in the figures 25 to 31 for each single element type. In order to reference these results they are plotted with the analytical results of FSDT and the experimental results.

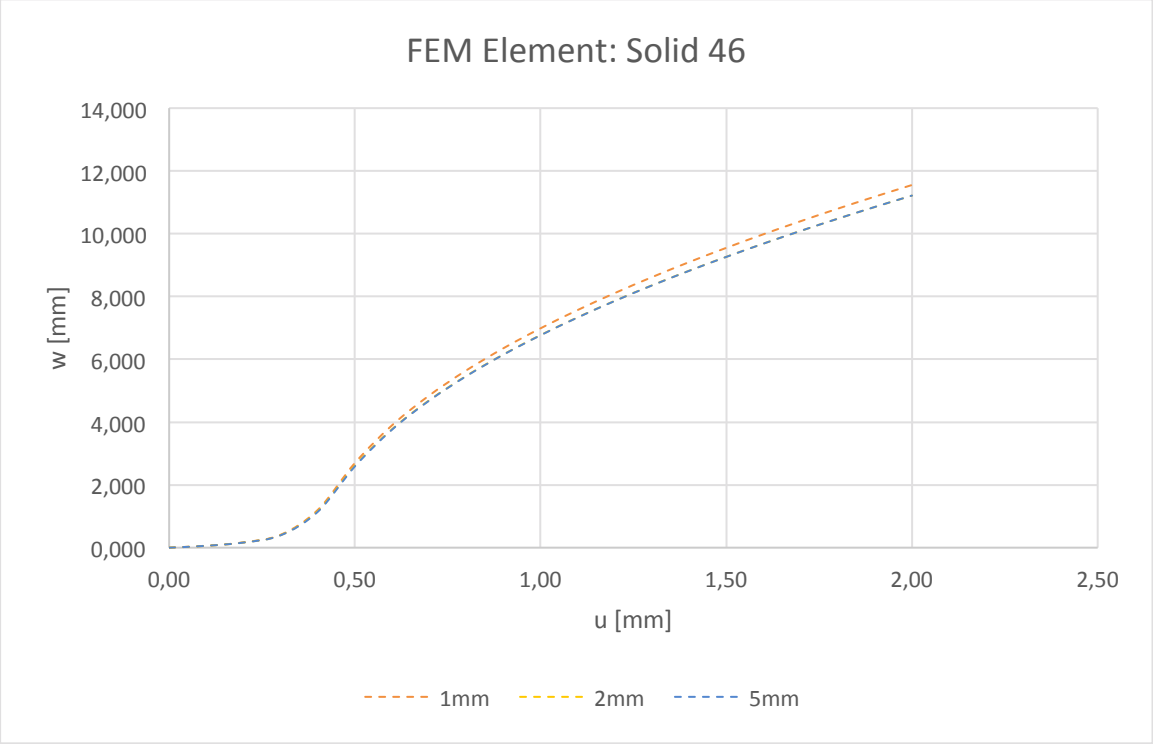

Figure 25: Solid 46 mesh size influence of deflection in x-direction.

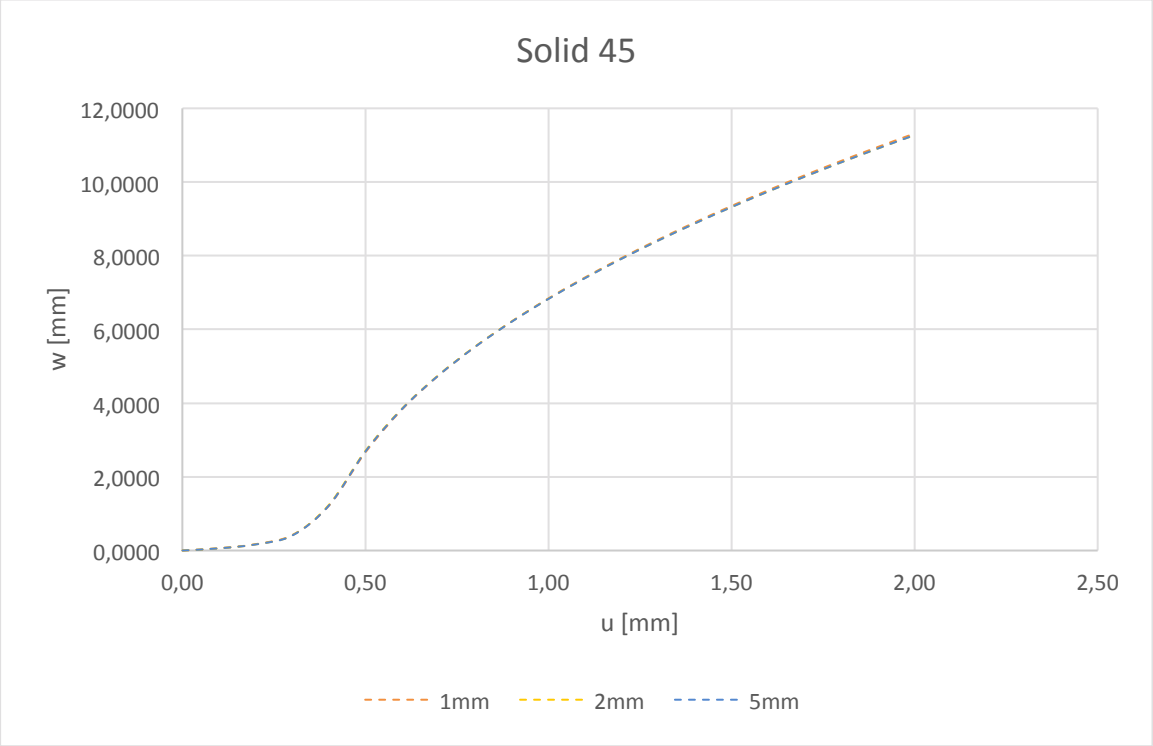

Figure 26: Solid 45 mesh size influence of deflection in x-direction.

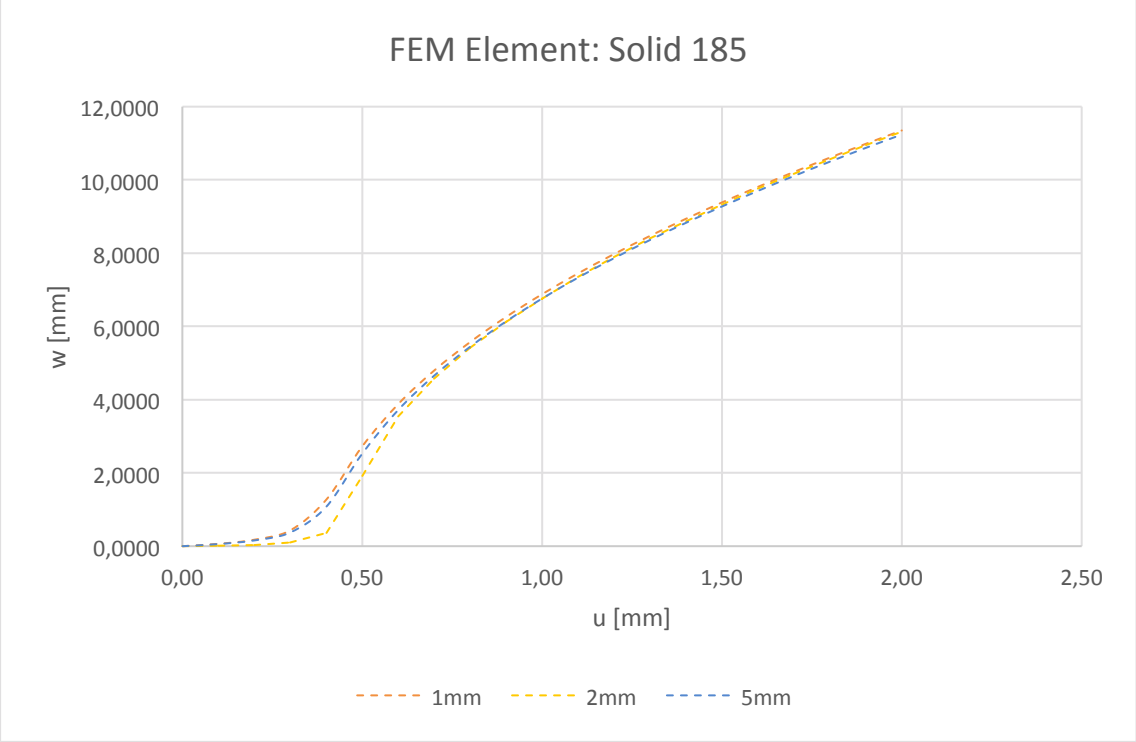

Figure 27: Solid 185 mesh size influence of deflection in x-direction.

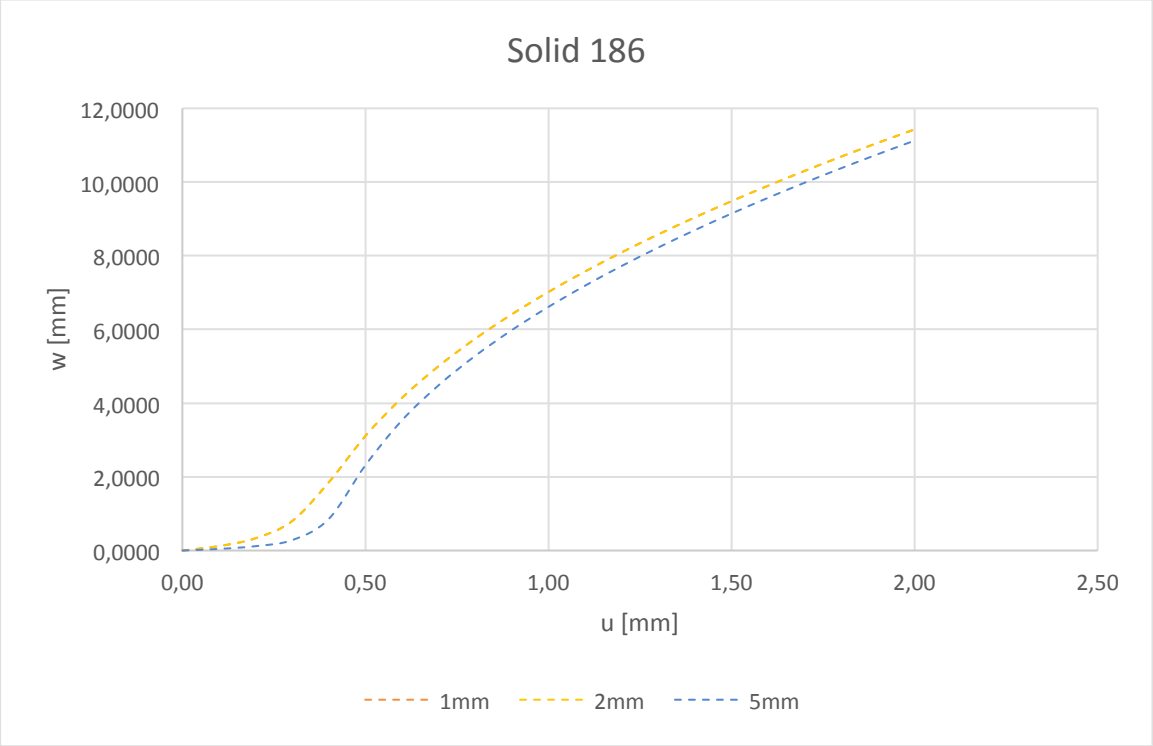

Figure 28: Solid 186 mesh size influence of deflection in x-direction.

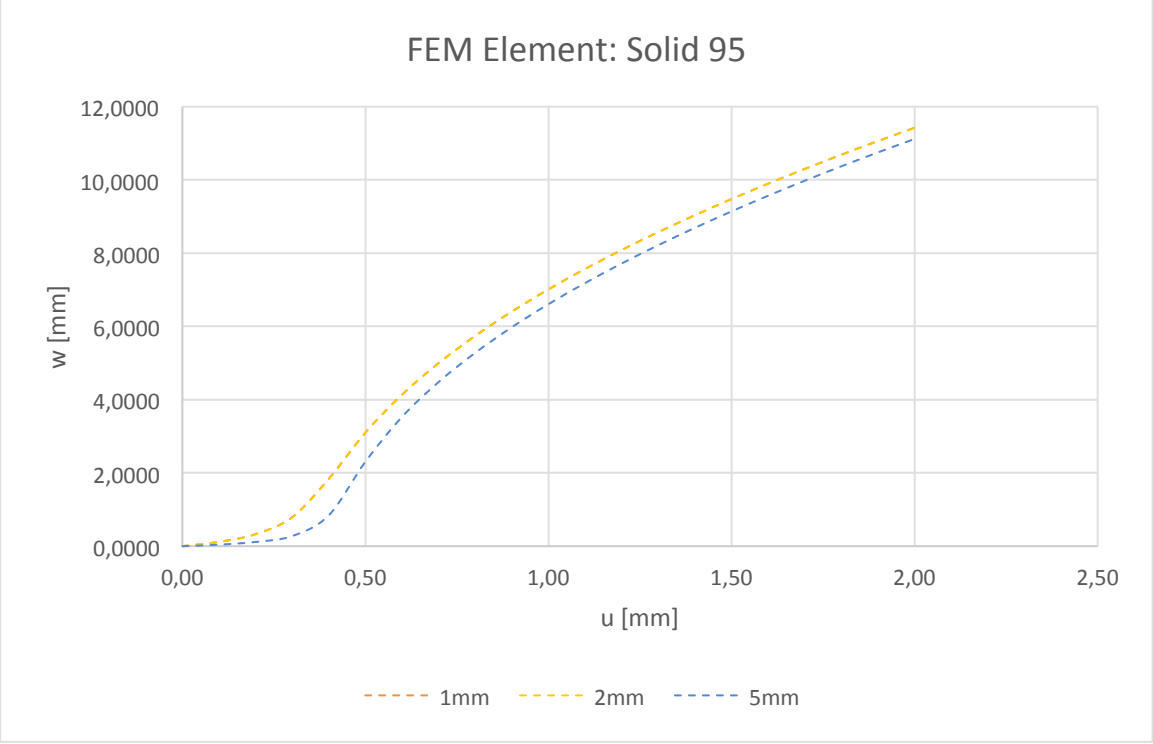

Figure 29: Solid 95 mesh size influence of deflection in x-direction.

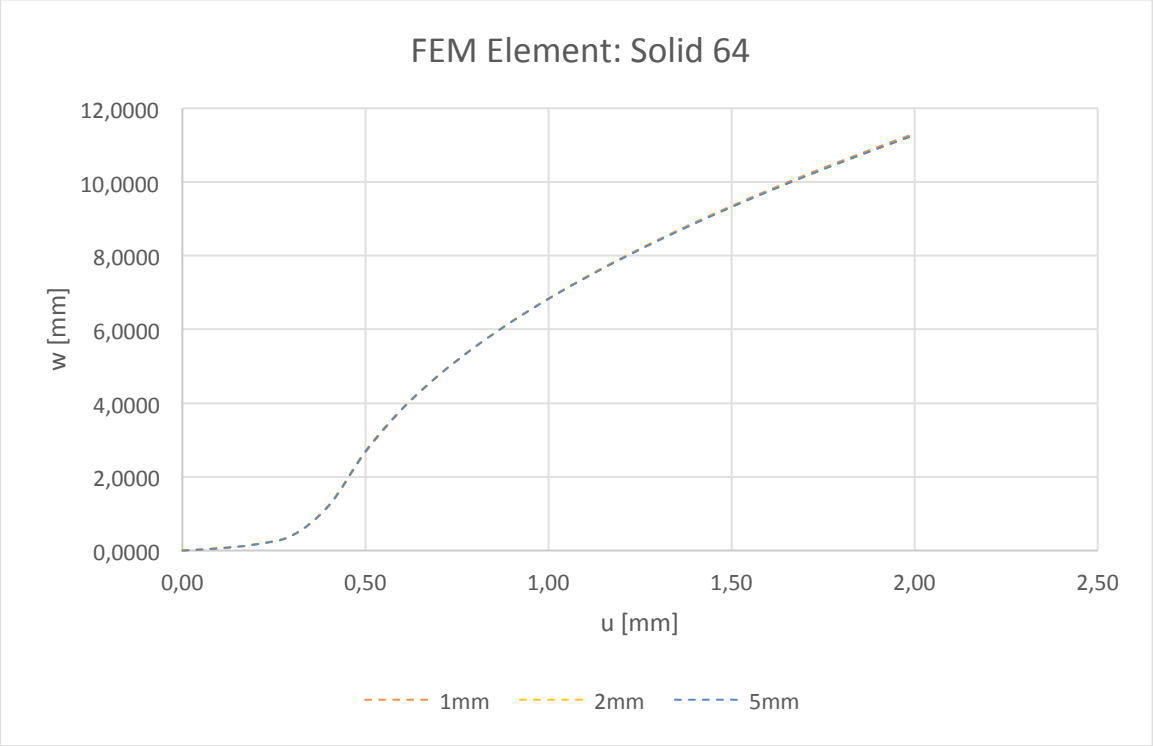

Figure 30: Solid 64 mesh size influence of deflection in x-direction.

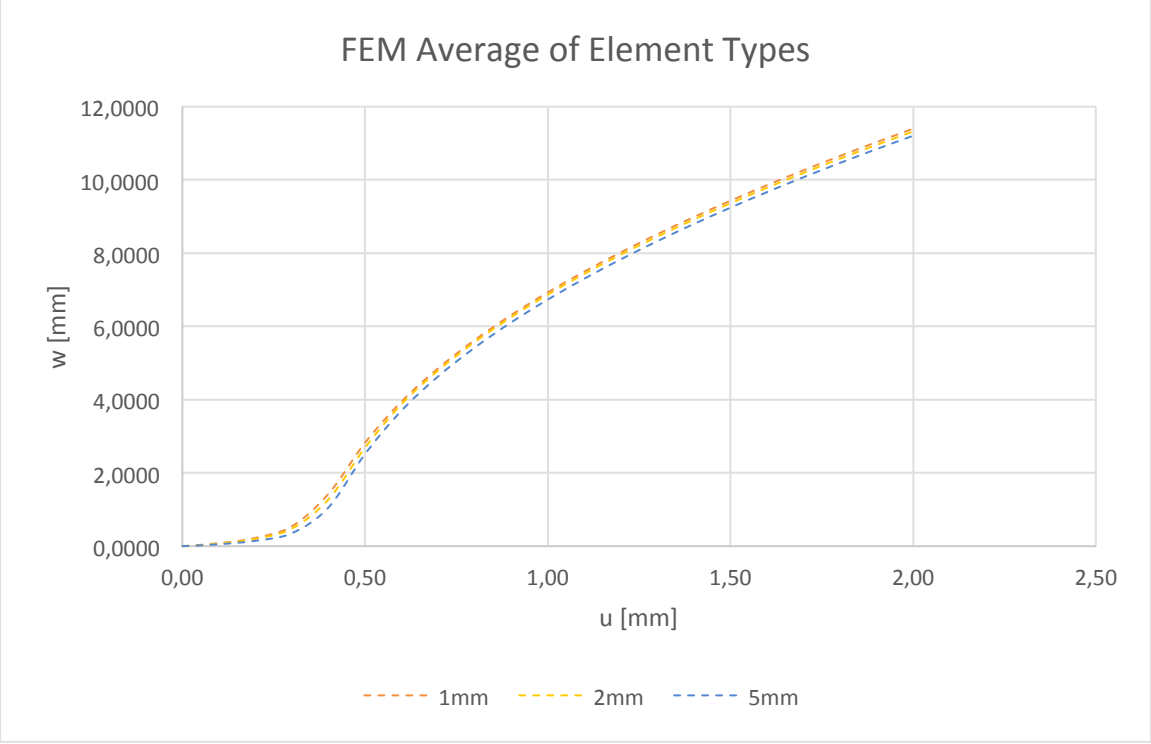

Figure 31: Average mesh size influence of deflection in x-direction.

6.3.2 Ansys mesh size Influence in x-direction and z-direction for Solid 45

Following a basic mesh size comparison in x-axis, a more detailed investigation is done on the example of the Solid 45 element. The results are presented in figure 32 and 33 for a mesh refinement in z- and x-direction respectively.

For mesh size comparison, it is chosen to be proven by the results of the out-of-plane deflection of a chosen node on the centre of the plane.

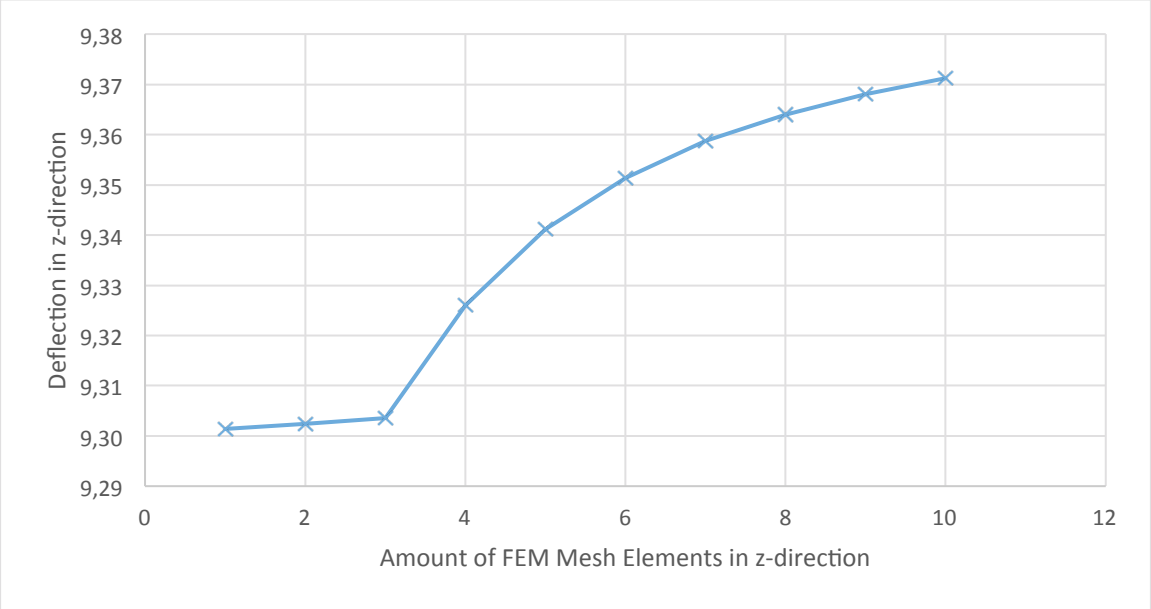

Figure 32: Results of mesh size variation in z-direction (t=5.31 mm, u = 1.5 mm).

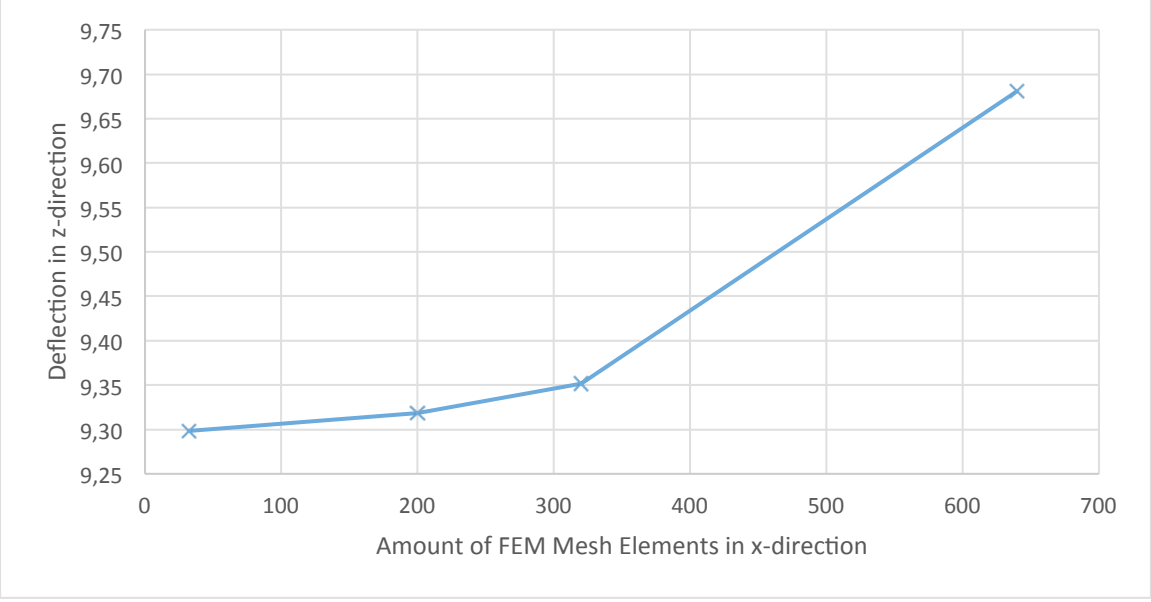

Figure 33: Results of mesh size variation in x-direction (t = 5.31 mm, u = 1.5 mm).

6.4 Discussion of Results

6.4.1 Analytical Buckling Analysis

All analytical calculations based on the developed *Maple* codes are performed successfully.

As the figures 22, 23 and 24 show, the plate theories behave related to plate thickness. While both theories predict pre- and post-buckling behaviour nicely, CLPT is underestimating deflection values slightly, especially for thicker plates, because it doesn't take shear forces into account.

For the plate thicknesses of 7.92 mm and 5.31 mm, the results of CLPT are slightly lower in terms of w-deflections than the FSDT. The discrepancy between those two theories increases with a higher plate thickness. This is nicely shown by the figures 22 and 23. This kind of behaviour of CLPT was expected since it is a plate theory for rather thin plates. Kirchhoff's CLPT doesn't include out-of-plane shear forces and is therefore rather useful for thin, shell-like plates. Mindlin improved this theory by taking shear forces into account in his first-order of shear theory. Therefore, his theory shall be more suitable for thicker plates, as well as for thin plates (see figure 24). The length over thickness ratios in x-direction of the three plates are 25.25, 37.66 and 80.32 for the plate thicknesses of 7.92, 5.31 and 2.59 mm respectively. A higher ratio should result in closer results of the two mentioned theories. If the ratio decreases, the results of CLPT loose accuracy while those of FSDT do not. The results of the two theories (figure 22 to 24) approve those assumptions perfectly. For instance, the results for the thin plate thickness of 2.49 mm (figure 24) of CLPT and FSDT are covering each other with high precision. The assumption of loss of accuracy for CLPT applied to thicker plates is reinforced by the relative errors in table 2. For the plate thicknesses of 2.49 and 5.31 mm the critical point of buckling initiation is predicted very accurate and equally, while they vary much more for the thickness of 7.92 mm.

An overestimated buckling initiation value, like in this case for CLPT, can be expected for a relatively thick plate. Results of strains (figures 25, 26 and 27) are directly related to the previously described w-deflections. Once again, the theories of CLPT and FSDT show similar behaviour for thin plate thickness as 2.49 mm (figure 27) and higher discrepancies for thicker plate thicknesses (figure 25 and 26). The same trend of the two theories related to plate thicknesses counts for the out-of-plane buckling shape comparisons in tables 3, 4 and 5.

6.4.2 Finite Element Buckling Analysis

The FEA was concluded with the software package of *Ansys* and based on the 3D element type Solid 46. Computation efficiency depends highly on the amount of elements and thus on the chosen mesh size. All numerical results show a smooth transition in between pre- and post-buckling. Further, all results show realistic magnitudes in terms of out-of-plane deflections and longitudinal strains.

6.4.3 Experimental Results

Practical experiments show typical pre- and post-buckling behaviour for all plate thicknesses. The specimen used for the practical experiments were of favourable quality, which reflects in the test results.

6.4.4 Comparison of Analytical, Numerical and Experimental Results

All three methods generally show roughly the same behaviour in terms of buckling pre- and post-buckling. Hence, none of the applied methods resulted in complete failure of buckling prediction. Comparing the three methods in more detail with each other, it is clear, that numerical results show a smoother, more realistic transition from pre- to post-buckling than the sudden change in the analytical results. For finite element computations, the buckling initiation is predicted to occur roughly at the same value of displacement as for FSDT for all of the three plate thicknesses. Finite element results predict pre- and post-buckling behaviour for all three plate thicknesses with roughly the same accuracy. The pre-buckling behaviour of *Ansys* for the plate thickness 7.92 mm is nicely covering the experimental results until the buckling initiation occurs earlier during the numerical computation. In terms of safety predictions, the critical buckling loads/displacement can be interpreted to be conservative for all FSDT, most CLPT and the finite element results. Even clearer is the over-prediction of displacement during the post-buckling part. For all applied methods, the post-buckling behaviour is predicted to occur under less end-shortening than during the practical experiment results. The results of compressive and tensile strains are directly related to displacements and thus showing the same behaviour of over predicting results conservatively. Similar to the out-of-plane displacements, the graphs of strains are roughly parallel to the experimental results. Once again, this shows a satisfactory prediction of the general behaviour although of higher magnitude.

6.4.5 Displacement Shape Comparison

The out-of-plane displacement shape comparison for the end-shortening value of u = 1.5 mm shows the best comparison for the medium plate thickness of 5.31 mm. The three graphs of FSDT, CLPT and *Ansys* overlap each other with high precision. With the same trigonometric displacement assumption function and amount of degrees of freedom for FSDT and CLPT, the two graphs are expected to be the same if the amplitude of the transverse deflection shape is the same. The displacement shape of *Ansys* approves the trigonometric approach since the graphs are covering each other without obvious differences.

6.4.6 Ansys: Element Type Comparison

An investigation on different element types in the finite element software of *Ansys* has been done to figure out the main differences, advantages, disadvantages and their suitability to composite plates. The elements included lower and higher order elements of the group of Solid 3D. Further,

some layered elements and some with a layered option were included in the investigation. The comparison of elements is implemented on the plate thickness of 5.31 mm. All computations for this comparison are done for three different mesh sizes in x-axis (1 mm, 2 mm and 5 mm).

The out-of-plane deflection comparison in the figures 28, 29 and 30 show all satisfying predictions of pre- and post-buckling behaviour. All element types predict especially the post buckling behaviour with high precision. This does also count for all three mesh sizes. Buckling initiation behaviour is slightly over predicted for the higher order element types of Solid 186 and 95. These elements have 20 nodes per element instead of 8 for the lower order elements. These higher order elements are supposed to be more accurate, since they do not tend as much to result in locking errors. However, they vary in highest scale from the average of all element types, from experimental results and from the results of FSDT. In addition, they are highly inefficient compared to lower order elements. For a mesh size of 2 mm in x-direction the element type Solid 185 under predicts buckling initiation compared to the average elements. For mesh sizes of 1 mm (figure 28) and 5 mm (figure 30) all element types show good results and only vary slightly.

Results of the out-of-plane deflections are directly related to the strains compressive and tensile strains. Figure 41, 42 and 43 build up the impression that all Solid 3D element types are capable of predicting behaviour of strain values with an exception for the mesh size of 2 mm.

Table 3, 4 and 5 present the out-of-plane deflection shape for a fix end-shortening value of all element types. The results show that the higher order elements of Solid 186 and Solid 95 are more affected by the size of the mesh than lower order elements regarding the transverse deflection shape.

6.4.7 Ansys: Mesh Size Comparison

In the first step of the mesh size analysis the mesh sizes are inspected for all element types in the direction of the x-axis for three mesh sizes (1 mm, 2 mm and 5 mm). Results of these computations are shown in the figures 25 to 31 regarding out-of-plane deflection amplitude, figures 37 to 43 regarding strains and in the tables 10 to 16 regarding transverse deflection shapes. The outcome of Solid 46 calculations shows that all three mesh sizes are resulting with similar precision (figure 25). Solid 45 shows barely varying results for all three mesh sizes, as well (figure 26). Solid 185 shows altering results for all three mesh sizes with increasing values for finer mesh sizes (figure 27). As already stated earlier, the higher order elements 186 and 95 show a higher influence of the mesh size in x-direction. Both element types show similar precision of results for element corner lengths of 1 mm and 2 mm, while results of the 5 mm mesh are varying exceptionally (see figure 28 and 29). Solid 46 is another element type that shows nearly no affection by the chosen mesh sizes (see figures 39 and 46) and high computation efficiency when compared with the average computation time. Figure 31 shows the average results of the mesh size analysis in x-direction of all elements. The general trend of all

elements combined show increasing deflection and strain results for finer mesh sizes than for coarser ones in x-direction. The results of the transverse deflections in table 10 to 16 present an equal trend for the element types as the out-of-plane deflections and strains.
In addition to the three analysed mesh sizes in x-direction for all element types a more detailed investigation is implanted on the chosen element type of Solid 45. Solid 45 is chosen for this investigation because it shows the best computation efficiency while its result precision is very close to the average of all elements.

The detailed investigations of the mesh size in regard of element type Solid 45 shows increasing magnitude of results with finer mesh sizes (see figure 32 and 33). Especially for very fine mesh sizes, both figures show a strong increase of result magnitude.

7 | CONCLUSION

7.1 Conclusion of Results

A broad investigation of analytical, numerical and experimental buckling analysis procedures including their influencing factors resulted in this thesis.

For the analytical approach the two widely known methods for thin and thick plates developed by Kirchhoff and Mindlin (CLPT and FSDT) have been applied to three different plate thicknesses of 7.92, 5.31 and 2.49 mm. The plate theories behave related to plate thickness. While both theories predict pre- and post-buckling behaviour nicely, CLPT is underestimating deflection values slightly compared to FSDT, especially for thicker plates, because it doesn't take shear forces into account.
The trigonometric displacement assumption functions combined with the FSDT plate theory show great computation efficiency paired with high precision results, especially regarding post-buckling behaviour and the critical buckling load. Further the Rayleigh-Ritz method in combination with the Newton-Raphson method show good results when compared with other results while being highly efficient.

Numerical calculations for the comparison with analytical and experimental results are achieved by applying the software of *Ansys* based on the layered Solid 3D element type SOLID 46. Once more, all three plates were modelled and calculated. Compared with the analytical methods of FSDT and CLPT they are highly inefficient. This is caused by the high number of elements of the

chosen mesh size and the fact that results are computed for more aspects than actually needed in this study. All numerical results are satisfactory as the graphs show typical pre- and post-buckling behaviour including a realistic transition.
Concluding the acquired knowledge of the buckling analysis approaches, we can say that the assumptions based on theories are confirmed by results of analytical and numerical approaches.
The finite element approach is the most precise approach regarding pre- and post-buckling behaviour. The second best of the three methods is the analytical method of FSDT. CLPT is not to be recommended for a buckling analysis unless it is only concerned with thin plates, where the length over thickness ratio is higher than circa 40.

To achieve higher certainty on experimental results, it is required to make more tests for each plate thickness. This is based on the fact that generally experimental test results are influenced by imperfections like imperfect bonding in between the plies or micro cracks in glass fibres in the laminated composite plates that can lead to lower buckling loads or delamination for instance. However, experimental results are on the secure side compared to analytical and finite element calculations because of their lower magnitude in deflections and strains.

A comparison of the transverse deflection shapes of analytical and numerical results show very similar results and thus reinforce the choice of trigonometric shape functions during analytical computations.

The Solid 3D element type and mesh comparison results in a recommendation of the lower element types of Solid 46, 45 and 64. All three element types are only slightly affected in their precision by the mesh refinement and highly computation efficient compared with the other element types. In addition to that they are close to the average results of all element types. This basically means that with those element types a very coarse mesh (e.g. 5 mm in x-direction) can be chosen without sacrificing much precision, while increasing computation efficiency considerably. Higher order element types as Solid 186 and 95 show a higher variance in results for different mesh sizes combined with a highly inefficient computation time compared to the average. Solid 185 is the only lower order element that shows higher affection of mesh size and is therefore not to be recommended. A mesh refinement in z-direction results in a strong increase in result magnitude but comes in cost of computation time.

The study shows, that the interaction of theoretical results and practical experiments is of utmost importance. This is caused by the undeniable connection in between them. Especially in composite material structures, practical experiments are recommended because of their special characteristics due to anisotropic behaviour and possible delamination.

The outcome of this thesis can be seen as a guide for some specific chosen techniques including an analytical program for buckling analysis of composite plates and as a comprehensive reference of some important details.

7.2 Limitations

Despite, well rounded acquired knowledge regarding composite plate buckling and its analyses, this study shows also some limitations that are to be pointed out.

The results theoretical analytical approaches of CLPT and FSDT are strongly dependent on the applied methods, shape functions and chosen amount of degrees of freedom. Even though, all of these variables are chosen according best possible knowledge, these methods are limited in their precision.
As the finite element type analysis and mesh refinement analysis have shown, results of a FEA are depending on these choices and precision varies throughout those variables. During the finite element type comparison the problem of reference values arose and it was chosen to compare results to average values instead of experimental values. This means that element types could only be compared with each other instead.
Since experimental results are lower in magnitude throughout this study, they are not the best reference values for theoretical results.

7.3 Future Work

With a profound knowledge in theoretical, numerical and analytical buckling analysis acquired by mathematicians and researchers over the last few centuries, it is nowadays a difficult task to push boundaries even further. Whereas, experimental test results are less investigated and can thus be improved easier compared to theory. Thus, it is recommended to gain more experimental results. Especially the amount of experiments for one specific plate type and thickness shall be increased, in order to achieve statistical certainty. Receiving plates from more than only one specimen supplier can achieve further improvements on experimental results. In doing so it could be possible to spot possible errors resulting from production processes.

The analytical approach could be further investigated and compared in terms of the applied methods. For instance the Galerkin method can be implemented together with the plate theories of CLPT and FSDT and compared with the present results of the Rayleigh-Ritz method. Another interesting comparison would be the correlation in between the shape assumption of trigonometric and polynomial functions.

BIBLIOGRAPHY

[1] Greene, E., (1999), *Marine Composites,* 2nd ed., Eric Greene Associates, Inc., ISBN: 0-9673692-0-7.

[2] Bhagwan, Argawal, D., Lawrence, Broutman, J., Chandrashekhara, K., (2006), *Analysis and Performance of Fibre Composites,* 3rd ed., John Wiley and Sons, ISBN: 978-0-471-26891-8

[3] http://www.boatinternational.com/yachts/editorial-features/encores-owners-learn-from-experience-in-their-second-alloy-sailing-yacht--26119 (15.04.2016)

[4] Szilard, Dr. -Ing.. P.E. R., (2004), *Theories and Applications of Plate Analysis: Classical, Numerical and Engineering Methods*, John Wiley & Sons, Inc..

[5] Pankajkumar, K., (2014), *Free Vibration and Buckling Behaviour of Laminated Composite Panels under Thermal and Mechanical Loading,* Department of Mechanical Engineering, National Institute of Technology Rourkela.

[6] Turvey, G.J., Marshall, I.H., (1995), *Buckling and Postbuckling of Composite Plates*, Chapman and Hall. DOI: 10.1007/978-94-011-1228-4.

[7] Xu, J., Zhao, Q., Qiao, P., (2013) *A Critical Review on Buckling and Post-Buckling Analysis of Composite Structures*, Vol 2, Issue 3, P 157 – 168.

[8] Reddy, J.N., (2003), *Mechanics of Laminated Composite Plates and Shells: Theory and Analysis*, 2nd ed., CRC Press, ISBN: 0-8493-1592-1.

[9] Kharazi, M., Ovesy H.R., Taghizadeh M., (2009), *Buckling of the composite laminates containing through-the-width delaminations using different plate theories*, Composite Structures, Vol. 92, P 1176 - 1183, DOI: 10.1016/j.compstruct.2009.10.019.

[10] Yang, Q., (2009), *Simplified Approaches to Buckling of Composite Plates*, Faculty of Mathematics and Natural Science, University of Oslo.

[11] Ovesy, H., Kharazi, M., Asghari Mooneghi M., (2010), *Buckling of Composite Laminates with Through-The-Width Delamination Using a Novel Layerwise Theory,* 2nd International Conference on Composites: Characterization, Fabrication and Application (CCFA-2), Iran.

[12] Ganapathi, M., Patel, B.P., (1998), *Postbuckling Behaviour of Anisotropic Laminated Composite Plates due to Shear Loading*, Defence Science Journal, Vol. 48, P 433 – 440.

[13] Roylance, D., (2001), *Finite Element Analysis,* Department of Material Science and Engineering, Massachusetts Institute of Technology.

[14] Leissa A., (1985), *Buckling of Laminated Composite Plates and Shells*, AF Wright Aeronautical Laboratories, Ohio State University.

[15] Dawe, D.J., Lam, Azizian, S.S.E., Z.G., (1992), *Non-linear Finite Strip Analysis of Rectangular Laminates under End-Shortening, using Classical Plate Theory*, Numerical Methods in Engineering, Vol. 35, Issue 5, P 1087 - 1110, DOI: 10.1002/nme.1620350510

[16] Barbero, E.J., (2010), *Introduction to Composite Materials Design*, 2nd ed., CRC Press.

[17] ANSYS, *ANSYS Mechanical APDL Element Reference.*

[18] http://www.eureka.im/3225.html

[19] Lee, H.P., Lim, S.P., (1991), *Free Vibration of Isotropic and Orthotropic Rectangular Plates with Partially Clamped Edges,* Department of Mechanical & Production Engineering, National University of Singapore.

[20] Kharghani, N. and Guedes Soares, C., (2015), *Influence of different parameters on the deflection of composite laminates containing through-the-width delamination using Layerwise HSDT*, Composite Structures, Vol. 132, P 341 – 349.

[21] Kharghani, N. and Guedes Soares, C., (2016), *Behavior of composite laminates with embedded delaminations*, Composite Structures Vol. 150, P. 226 – 239.

A | APPENDIX

A.1 Buckling Analysis Results

A.1.1 Out-of-plane buckling shape comparison

The following plots present the out-of-plane displacement shapes for each plate thickness over the entire plate length in x direction (see table 3, 4 and 5). The results of CLPT, FSDT and *Ansys* are presented.

Table 3: Out-of-plane transverse buckling shapes for t = 7.92 mm

x	ASNYS	CLPT	FSDT
0	0,000	0,000	0,000
10	0,214	0,151	0,170
20	0,707	0,588	0,665
30	1,451	1,270	1,436
40	2,375	2,128	2,407
50	3,398	3,080	3,483
60	4,422	4,032	4,559
70	5,344	4,891	5,530
80	6,078	5,572	6,301
90	6,551	6,010	6,795
100	6,716	6,160	6,966
110	6,551	6,010	6,795
120	6,078	5,572	6,301
130	5,344	4,891	5,530
140	4,422	4,032	4,559
150	3,398	3,080	3,483
160	2,375	2,128	2,407
170	1,451	1,270	1,436
180	0,707	0,588	0,665
190	0,214	0,151	0,170
200	0,000	0,000	0,000

Table 4: Out-of-plane transverse buckling shapes for t = 5.31 mm

x	ASNYS	CLPT	FSDT
0	0,000	0,000	0,000
10	0,279	0,279	0,227
20	0,972	0,972	0,887
30	2,010	2,010	1,915
40	3,292	3,292	3,209
50	4,705	4,705	4,645
60	6,114	6,114	6,080
70	7,380	7,380	7,375
80	8,388	8,388	8,402
90	9,037	9,037	9,062
100	9,264	9,264	9,289
110	9,037	9,037	9,062
120	8,388	8,388	8,402
130	7,381	7,380	7,375
140	6,115	6,114	6,080
150	4,706	4,705	4,645
160	3,293	3,292	3,209
170	2,011	2,010	1,915
180	0,972	0,972	0,887
190	0,279	0,279	0,227
200	0,000	0,000	0,000

Table 5: Out-of-plane transverse buckling shapes for t = 2.49 mm

x	ASNYS	CLPT	FSDT
0	0,000	0,000	0,000
10	0,326	0,261	0,261
20	1,185	1,017	1,017
30	2,442	2,194	2,195
40	3,956	3,678	3,680
50	5,588	5,323	5,325
60	7,188	6,967	6,971
70	8,604	8,451	8,455
80	9,720	9,629	9,634
90	10,438	10,385	10,390
100	10,688	10,645	10,651
110	10,438	10,385	10,390
120	9,720	9,629	9,634

130	8,604	8,451	8,455
140	7,188	6,967	6,971
150	5,588	5,323	5,325
160	3,956	3,678	3,680
170	2,442	2,194	2,195
180	1,185	1,017	1,017
190	0,326	0,261	0,261
200	0,000	0,000	0,000

A.2 Ansys Element Analysis

Table 6: Standard Deviation of w-deflections.

u	5mm	2mm	1mm
0,00	0,0000	0,0000	0,0000
0,10	0,2023	0,0369	0,0271
0,20	0,0217	0,1026	0,0755
0,30	0,0556	0,2442	0,1780
0,40	0,1554	0,4969	0,2960
0,50	0,1571	0,3943	0,1990
0,60	0,1286	0,2073	0,1366
0,70	0,1134	0,1568	0,1072
0,80	0,1038	0,1271	0,0913
0,90	0,0969	0,1124	0,0824
1,00	0,0914	0,1033	0,0773
1,10	0,0870	0,0960	0,0748
1,20	0,0833	0,0907	0,0735
1,30	0,0800	0,0869	0,0734
1,40	0,0771	0,0842	0,0741
1,50	0,0746	0,0822	0,0750
1,60	0,0722	0,0808	0,0761
1,70	0,0701	0,0799	0,0775
1,80	0,0681	0,0793	0,0791
1,90	0,0663	0,0789	0,0806
2,00	0,0646	0,0788	0,0821

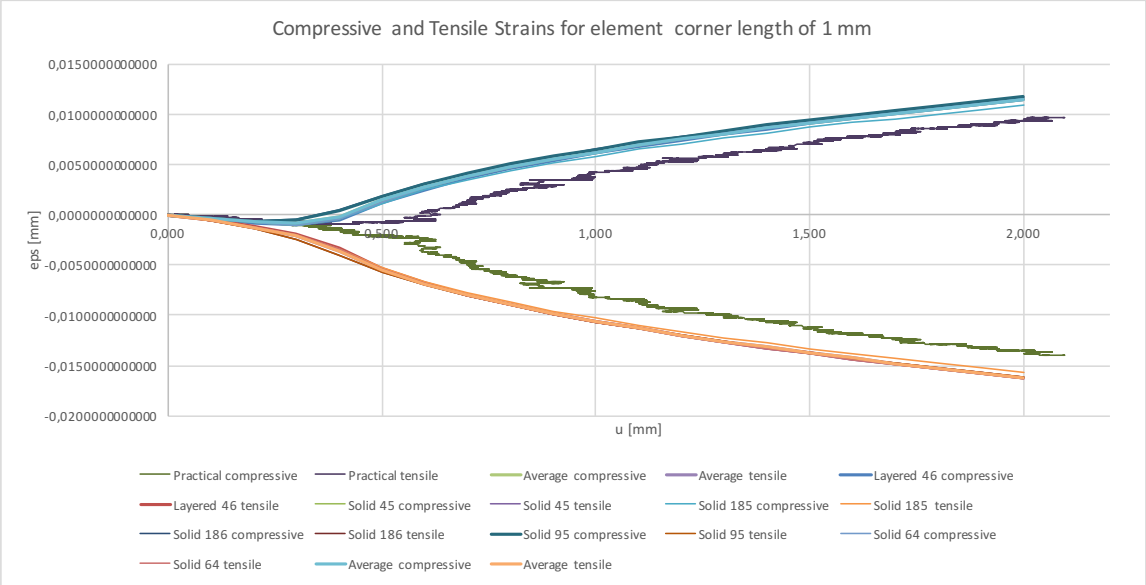

Figure 34: Strains for element corner length of 1 mm in x-direction (t = 5.31 mm).

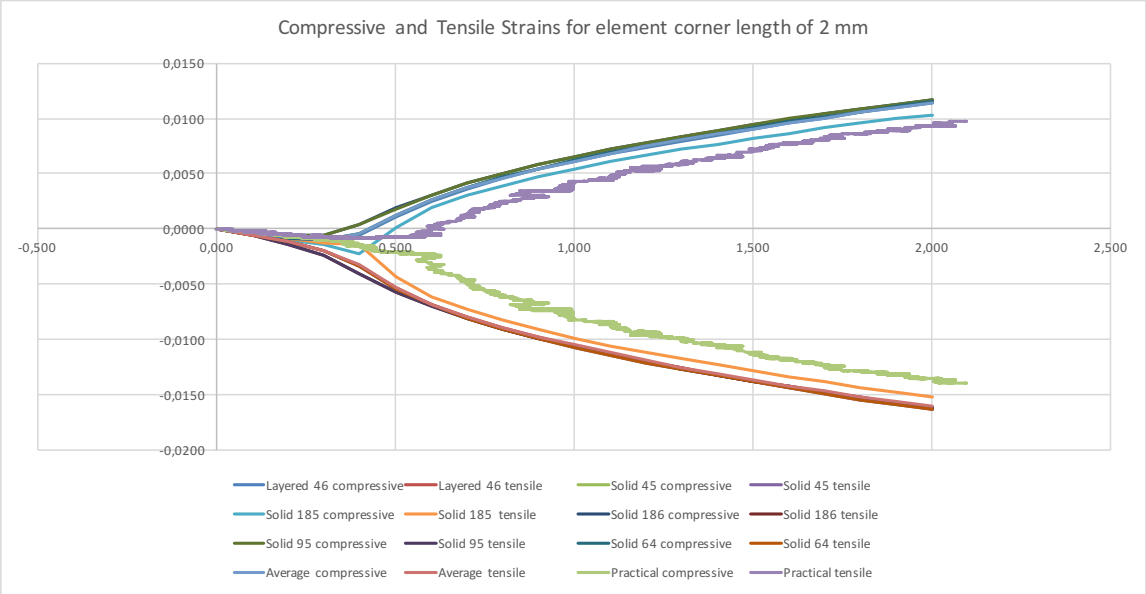

Figure 35: Strains for element corner length of 2 mm in x-direction (t = 5.31 mm).

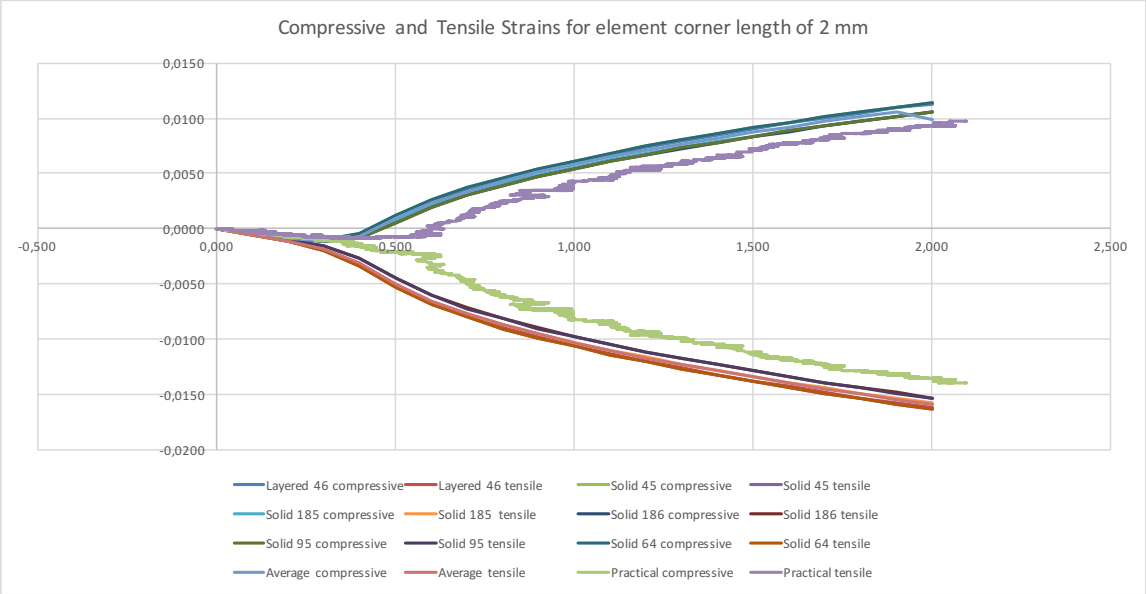

Figure 36: Strains for element corner length of 5 mm in x-direction (t = 5.31 mm).

Table 7: Deflection shape for element corner length of 1 mm.

x	Solid 46	Solid 45	Solid 185	Solid 186	Solid 95	Solid64	Average
0,0	0,000	0,000	0,000	0,000	0,000	0,000	0,000
10,0	0,279	0,325	0,331	0,302	0,302	0,281	0,303
20,0	0,972	1,065	1,080	1,034	1,033	0,978	1,027
30,0	2,010	2,134	2,152	2,118	2,116	2,024	2,092
40,0	3,292	3,431	3,454	3,436	3,434	3,314	3,394
50,0	4,705	4,844	4,871	4,878	4,876	4,735	4,818
60,0	6,114	6,244	6,274	6,311	6,309	6,152	6,234
70,0	7,380	7,496	7,528	7,585	7,583	7,426	7,500
80,0	8,388	8,489	8,522	8,597	8,595	8,440	8,505
90,0	9,037	9,128	9,161	9,250	9,247	9,093	9,153
100,0	9,264	9,351	9,384	9,481	9,478	9,321	9,380
110,0	9,037	9,130	9,163	9,250	9,247	9,093	9,153
120,0	8,388	8,492	8,525	8,597	8,595	8,440	8,506
130,0	7,380	7,501	7,533	7,585	7,583	7,427	7,501
140,0	6,114	6,250	6,280	6,311	6,309	6,153	6,236
150,0	4,705	4,850	4,877	4,878	4,876	4,736	4,820
160,0	3,292	3,436	3,460	3,436	3,434	3,315	3,396
170,0	2,010	2,138	2,157	2,118	2,116	2,024	2,094
180,0	0,972	1,068	1,080	1,034	1,033	0,979	1,028
190,0	0,279	0,326	0,332	0,302	0,302	0,281	0,303
200,0	0,000	0,000	0,000	0,000	0,000	0,000	0,000

Table 8: Deflection shape for element corner length of 2 mm.

x	Solid 46	Solid 45	Solid 185	Solid 186	Solid 95	Solid64	Average
0	0,000	0.0000	0,000	0.0000	0.0000	0,000	0,000
10	0,279	0,281	0,271	0,301	0,301	0,281	0,286
20	0,971	0,978	0,951	1,033	1,032	0,978	0,991
30	2,009	2,023	1,957	2,116	2,114	2,023	2,040
40	3,292	3,313	3,204	3,434	3,431	3,313	3,331
50	4,704	4,734	4,585	4,876	4,873	4,734	4,751
60	6,113	6,152	5,978	6,309	6,304	6,152	6,168
70	7,380	7,426	7,256	7,583	7,579	7,426	7,441
80	8,387	8,439	8,299	8,595	8,591	8,439	8,458
90	9,037	9,093	9,010	9,248	9,243	9,093	9,120
100	9,263	9,321	9,319	9,479	9,474	9,321	9,363
110	9,037	9,093	9,010	9,248	9,243	9,093	9,120
120	8,387	8,439	8,299	8,595	8,591	8,439	8,458
130	7,380	7,426	7,256	7,583	7,579	7,426	7,441
140	6,113	6,152	5,978	6,309	6,304	6,152	6,168
150	4,704	4,734	4,585	4,876	4,873	4,734	4,751
160	3,292	3,313	3,204	3,434	3,431	3,313	3,331
170	2,009	2,023	1,957	2,116	2,114	2,023	2,040
180	0,971	0,978	0,951	1,033	1,032	0,978	0,991
190	0,279	0,281	0,271	0,301	0,301	0,281	0,286
200	0.0000	0.0000	0,000	0,000	0.0000	0,000	0,000

Table 9: Deflection shape for element corner length of 5 mm.

x	Solid 46	Solid 45	Solid 185	Solid 186	Solid 95	Solid64	Average
0	0,000	0,000	0,000	0.0000	0,000	0,000	0,000
10	0,277	0,279	0,276	0,302	0,639	0,279	0,342
20	0,969	0,976	0,968	1,080	1,555	0,976	1,088
30	2,007	2,021	2,007	2,143	2,728	2,021	2,154
40	3,289	3,311	3,292	3,413	4,059	3,311	3,446
50	4,701	4,732	4,707	4,781	5,434	4,732	4,848
60	6,110	6,150	6,118	6,129	6,730	6,150	6,231
70	7,378	7,425	7,388	7,338	7,834	7,425	7,464
80	8,386	8,439	8,397	8,301	8,646	8,439	8,435
90	9,035	9,093	9,048	8,933	9,095	9,093	9,049
100	9,261	9,320	9,274	9,177	9,140	9,320	9,249
110	9,035	9,093	9,048	8,933	9,095	9,093	9,049
120	8,386	8,439	8,397	8,301	8,646	8,439	8,435
130	7,378	7,425	7,388	7,338	7,834	7,425	7,464

140	6,110	6,150	6,118	6,129	6,730	6,150	6,231
150	4,701	4,732	4,707	4,781	5,434	4,732	4,848
160	3,289	3,311	3,292	3,413	4,059	3,311	3,446
170	2,007	2,021	2,007	2,143	2,728	2,021	2,154
180	0,969	0,976	0,968	1,080	1,555	0,976	1,088
190	0,277	0,279	0,276	0,302	0,639	0,279	0,342
200	0.0000	0,000	0,000	0.0000	0,000	0,000	0,000

A.3 Ansys Mesh Size Analysis

A.3.1 Strain comparison of element types

The strain results for varying mesh sizes in x-direction are plotted in the figures 37-43 for each single element type. In order to reference these results they are plotted with the analytical results the experimental results.

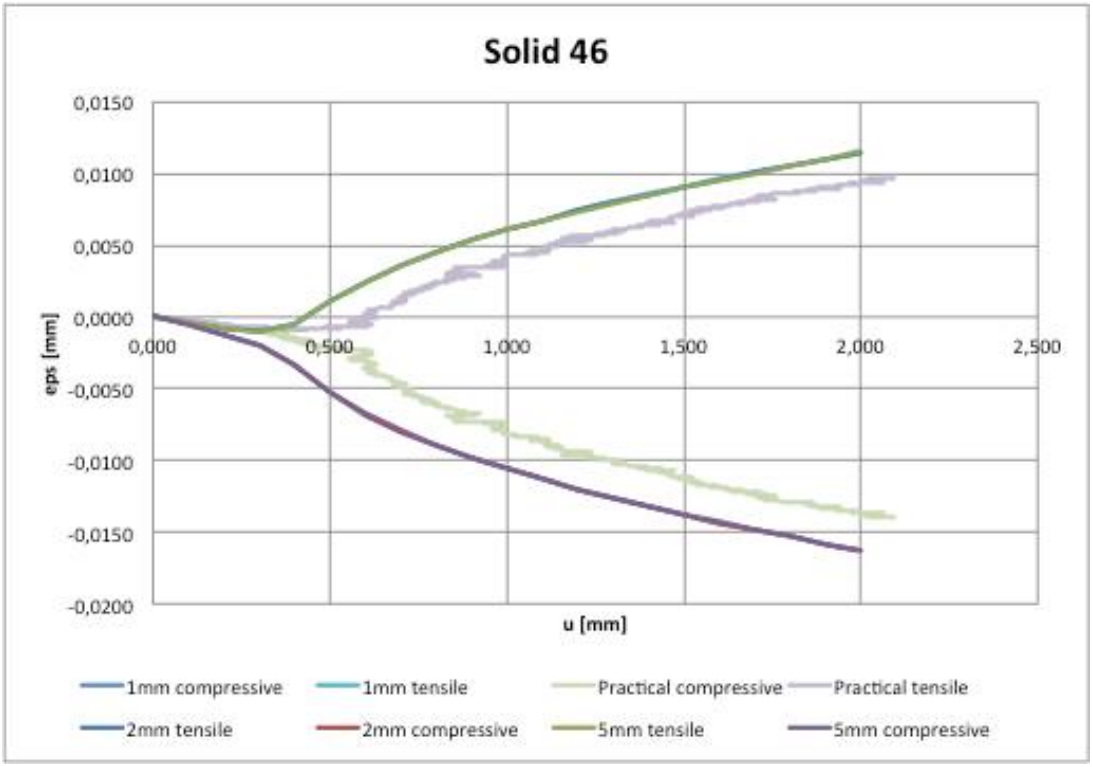

Figure 37: Solid 46 mesh size influence of strain in x-direction.

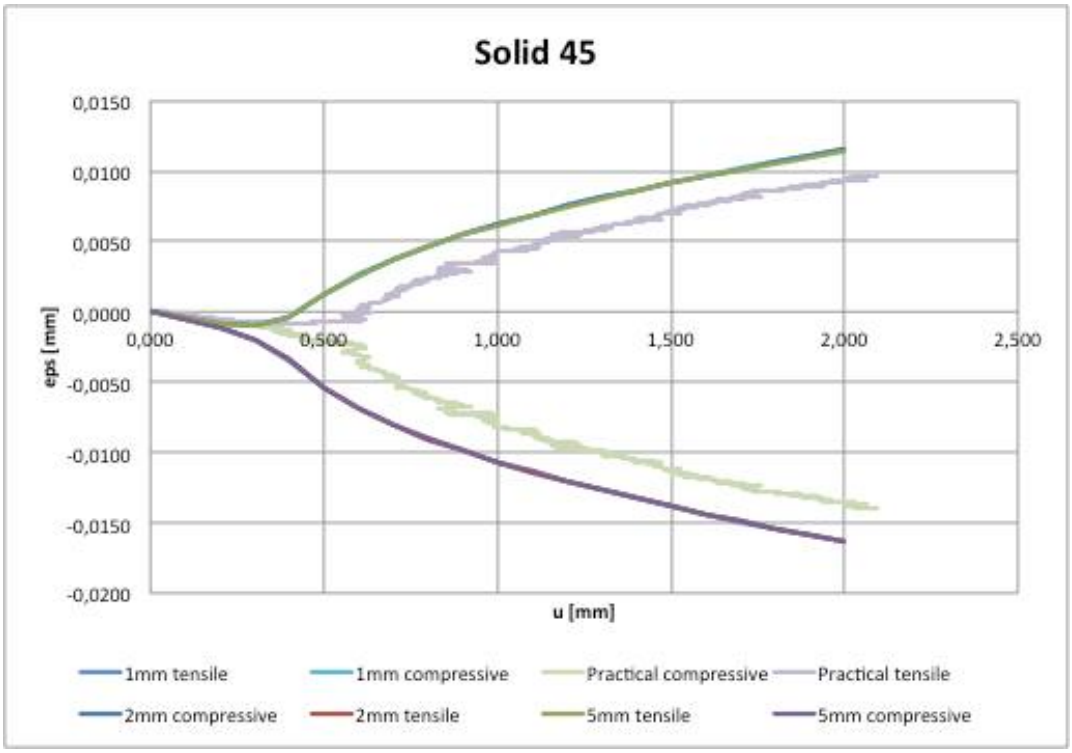

Figure 38: Solid 45 mesh size influence of strain in x-direction.

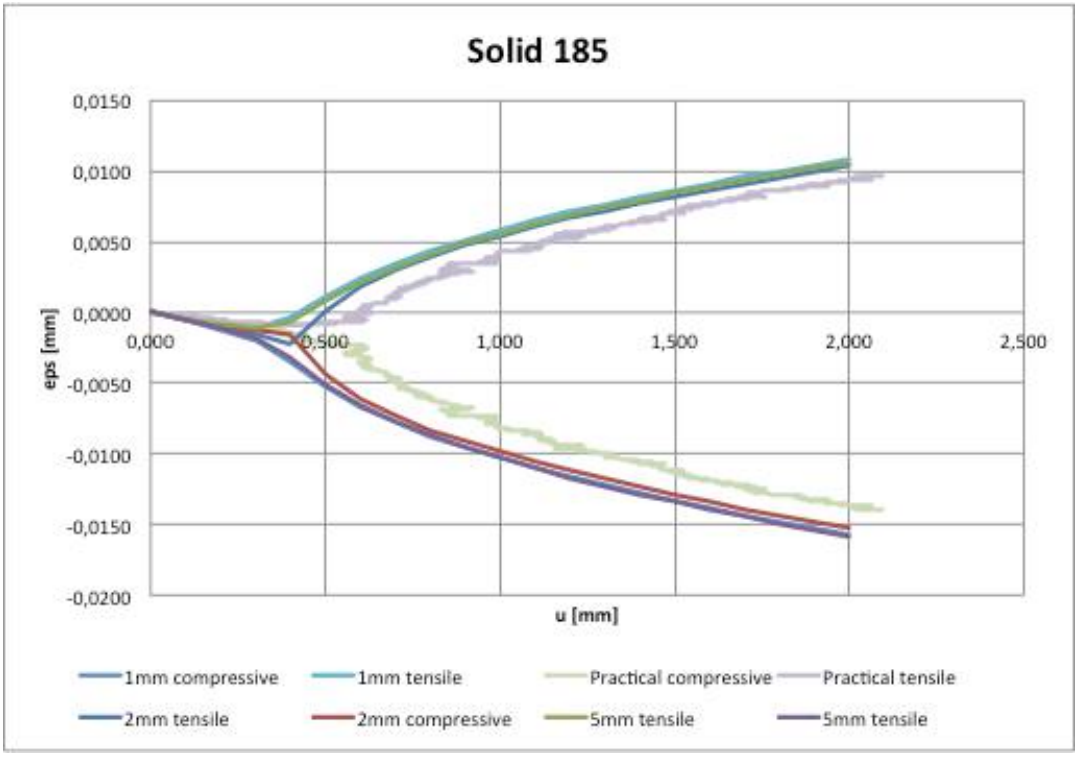

Figure 39: Solid 185 mesh size influence of strain in x-direction.

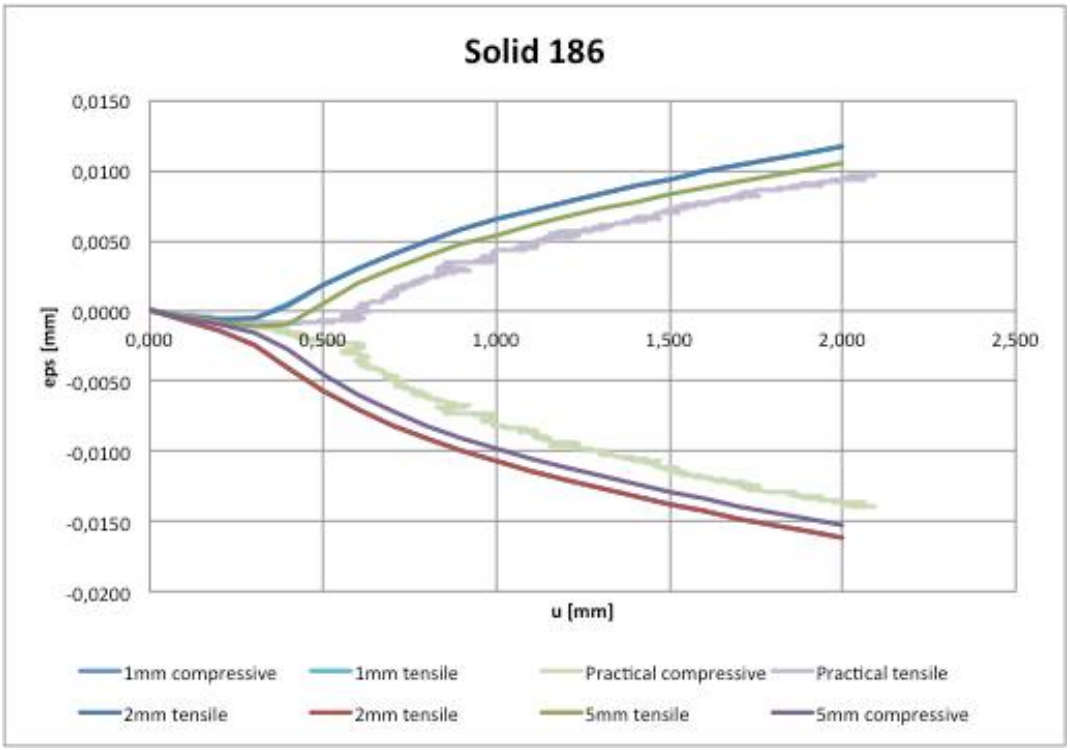

Figure 40: Solid 186 mesh size influence of strain in x-direction.

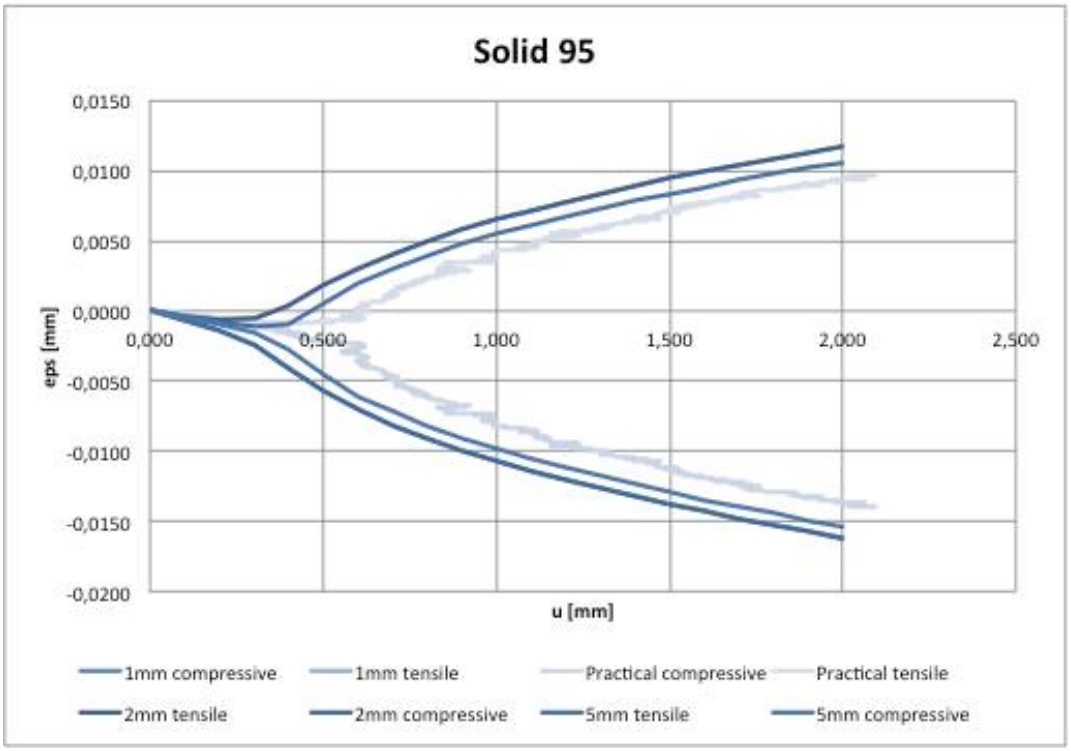

Figure 41: Solid 95 mesh size influence of strain in x-direction.

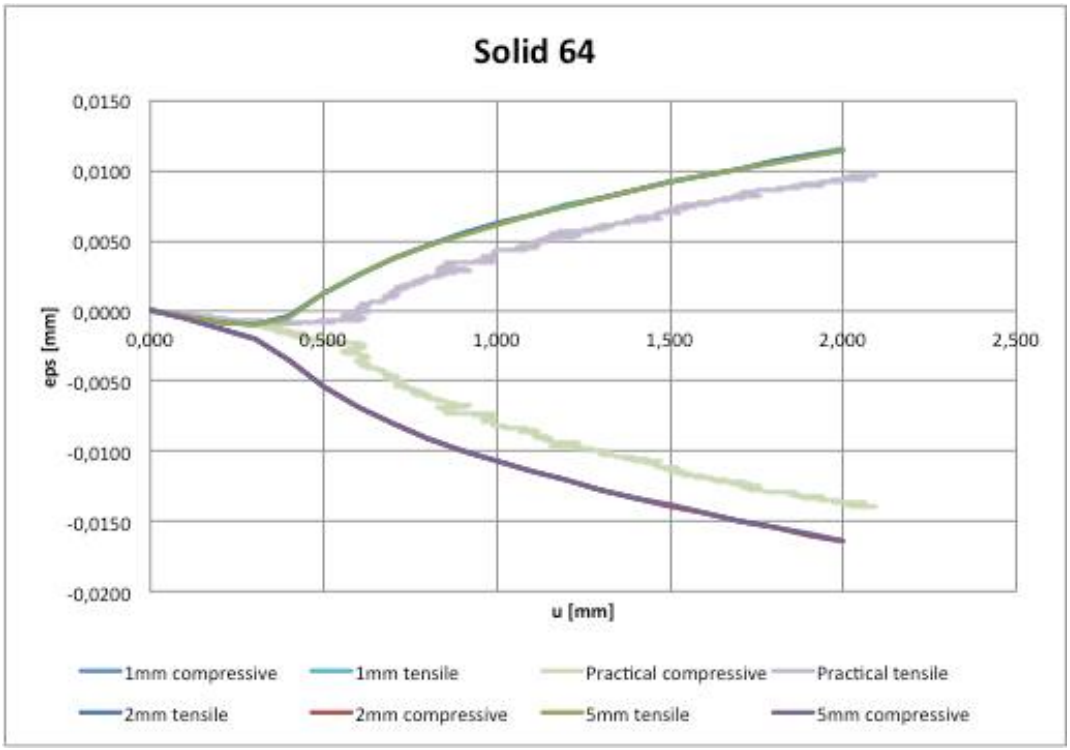

Figure 42: Solid 64 mesh size influence of strain in x-direction.

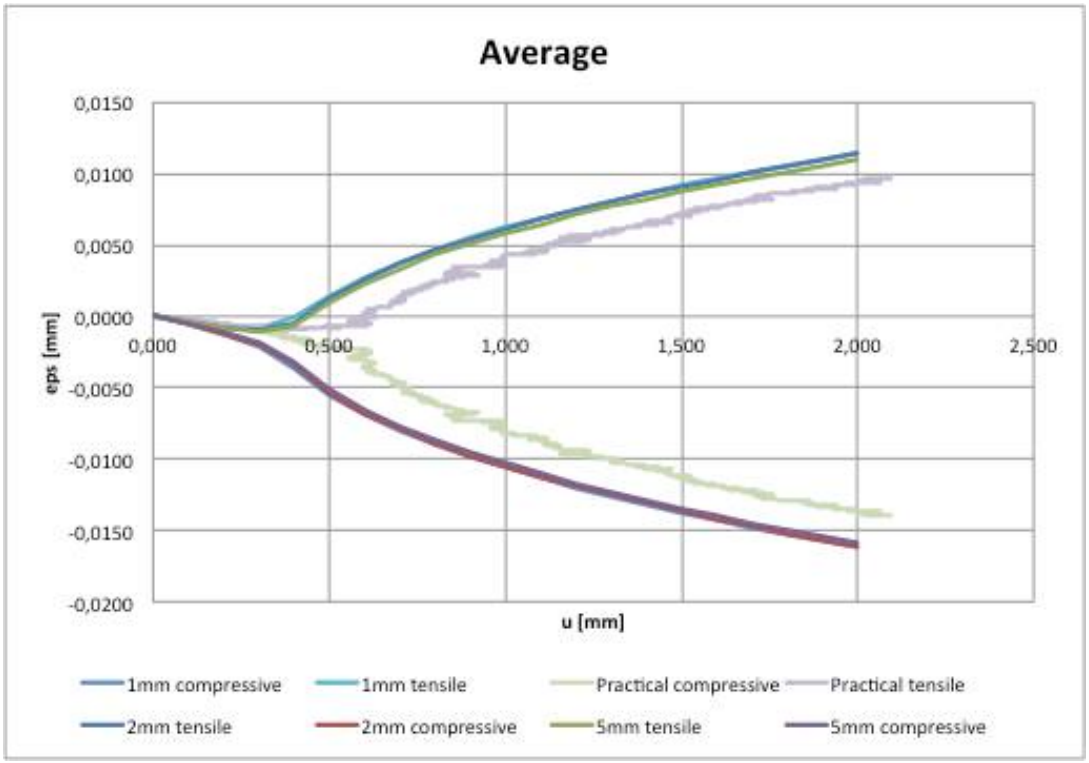

Figure 43: Average element mesh size influence of strain in x-direction.

A.3.2 Out-of-plane deflection shape comparison

The resulting out-of-plane shapes of each element type for a fixed end-shortening value of u = 1.5 mm. Equal to the previous results the varied mesh size in x-direction ranges from 1 mm over 2 mm and 5 mm element corner length. The results are presented in the tables number 10-16.

Table 10: Solid 46 w-deflection shape.

x	5mm	2mm	1mm
0	0,0000	0,0000	0,0000
10	0,2773	0,2786	0,2789
20	0,9694	0,9713	0,9717
30	2,0067	2,0094	2,0102
40	3,2889	3,2918	3,2924
50	4,7011	4,7041	4,7046
60	6,1104	6,1134	6,1141
70	7,3777	7,3799	7,3803
80	8,3855	8,3872	8,3875
90	9,0352	9,0365	9,0369
100	9,2613	9,2629	9,2636
110	9,0352	9,0365	9,0369
120	8,3855	8,3872	8,3875
130	7,3777	7,3799	7,3803
140	6,1104	6,1134	6,1141
150	4,7011	4,7041	4,7046
160	3,2889	3,2918	3,2924
170	2,0067	2,0094	2,0102
180	0,9694	0,9713	0,9717
190	0,2773	0,2786	0,2789
200	0.0000	0.0000	0,0000

Table 11: Solid 45 w-deflection shape.

x	5mm	2mm	1mm
0	0,0000	0.0000	0,0000
10	0,2793	0,2806	0,3247
20	0,9764	0,9780	1,0649
30	2,0206	2,0228	2,1341
40	3,3109	3,3132	3,4309
50	4,7318	4,7340	4,8439
60	6,1496	6,1517	6,2442

70	7,4246	7,4258	7,4961
80	8,4387	8,4393	8,4889
90	9,0925	9,0927	9,1278
100	9,3202	9,3205	9,3513
110	9,0925	9,0927	9,1297
120	8,4387	8,4393	8,4923
130	7,4246	7,4258	7,5008
140	6,1496	6,1517	6,2497
150	4,7318	4,7340	4,8496
160	3,3109	3,3132	3,4362
170	2,0206	2,0228	2,1383
180	0,9764	0,9780	1,0676
190	0,2793	0,2806	0,3258
200	0,0000	0.0000	0,0000

Table 12: Solid 185 w-deflection shape.

x	5mm	2mm	1mm
0	0,0000	0,0000	0,0000
10	0,2763	0,2714	0,3308
20	0,9684	0,9512	1,0799
30	2,0073	1,9565	2,1521
40	3,2920	3,2036	3,4542
50	4,7067	4,5850	4,8712
60	6,1182	5,9779	6,2740
70	7,3877	7,2555	7,5278
80	8,3972	8,2990	8,5215
90	9,0479	9,0095	9,1609
100	9,2742	9,3185	9,3844
110	9,0479	9,0095	9,1628
120	8,3972	8,2990	8,5250
130	7,3877	7,2555	7,5326
140	6,1182	5,9779	6,2797
150	4,7067	4,5850	4,8771
160	3,2920	3,2036	3,4597
170	2,0073	1,9565	2,1565
180	0,9684	0,9512	1,0799
190	0,2763	0,2714	0,3320
200	0,0000	0,0000	0,0000

Table 13: Solid 186 w-deflection shape.

x	5mm	2mm	1mm
0	0.0000	0.0000	0,0000
10	0,3024	0,3014	0,3018
20	1,0798	1,0330	1,0339
30	2,1434	2,1161	2,1178
40	3,4127	3,4341	3,4360
50	4,7810	4,8762	4,8784
60	6,1289	6,3085	6,3111
70	7,3380	7,5830	7,5852
80	8,3012	8,5953	8,5974
90	8,9328	9,2481	9,2500
100	9,1767	9,4792	9,4814
110	8,9328	9,2481	9,2500
120	8,3012	8,5953	8,5974
130	7,3380	7,5830	7,5852
140	6,1289	6,3085	6,3111
150	4,7810	4,8762	4,8784
160	3,4127	3,4341	3,4360
170	2,1434	2,1161	2,1178
180	1,0798	1,0330	1,0339
190	0,3024	0,3014	0,3018
200	0.0000	0,0000	0,0000

Table 14: Solid 95 w-deflection shape.

x	5mm	2mm	1mm
0	0,0000	0.0000	0,0000
10	0,6394	0,3009	0,3015
20	1,5552	1,0317	1,0332
30	2,7278	2,1137	2,1164
40	4,0592	3,4313	3,4344
50	5,4338	4,8728	4,8764
60	6,7303	6,3042	6,3086
70	7,8339	7,5787	7,5828
80	8,6464	8,5906	8,5949
90	9,0953	9,2432	9,2474
100	9,1404	9,4738	9,4784
110	9,0953	9,2432	9,2474
120	8,6464	8,5906	8,5949
130	7,8339	7,5787	7,5828

140	6,7303	6,3042	6,3086
150	5,4338	4,8728	4,8764
160	4,0592	3,4313	3,4344
170	2,7278	2,1137	2,1164
180	1,5552	1,0317	1,0332
190	0,6394	0,3009	0,3015
200	0,0000	0.0000	0,0000

Table 15: Solid 64 w-deflection shape.

x	5mm	2mm	1mm
0	0,0000	0,0000	0,0000
10	0,2793	0,2806	0,2808
20	0,9764	0,9780	0,9783
30	2,0206	2,0228	2,0235
40	3,3109	3,3132	3,3137
50	4,7318	4,7340	4,7345
60	6,1496	6,1517	6,1524
70	7,4246	7,4258	7,4262
80	8,4387	8,4393	8,4397
90	9,0925	9,0927	9,0930
100	9,3202	9,3205	9,3212
110	9,0925	9,0927	9,0934
120	8,4387	8,4393	8,4403
130	7,4246	7,4258	7,4270
140	6,1496	6,1517	6,1533
150	4,7318	4,7340	4,7355
160	3,3109	3,3132	3,3146
170	2,0206	2,0228	2,0242
180	0,9764	0,9780	0,9787
190	0,2793	0,2806	0,2809
200	0,0000	0,0000	0,0000

Table 16: Average element w-deflection shape.

x	5mm	2mm	1mm
0	0,0000	0,0000	0,0000
10	0,3423	0,2856	0,3031
20	1,0876	0,9905	1,0270
30	2,1544	2,0402	2,0924

40	3,4458	3,3312	3,3936
50	4,8477	4,7510	4,8182
60	6,2312	6,1679	6,2341
70	7,4644	7,4415	7,4997
80	8,4346	8,4585	8,5050
90	9,0494	9,1205	9,1527
100	9,2488	9,3626	9,3801
110	9,0494	9,1205	9,1534
120	8,4346	8,4585	8,5062
130	7,4644	7,4415	7,5015
140	6,2312	6,1679	6,2361
150	4,8477	4,7510	4,8203
160	3,4458	3,3312	3,3956
170	2,1544	2,0402	2,0939
180	1,0876	0,9905	1,0275
190	0,3423	0,2856	0,3035
200	0,0000	0,0000	0,0000